CHARACTERIZATION OF SURFACE MICROTOPOGRAPHY AND DETERMINATION OF HYDROTOPOGRAPHIC PROPERTIES

A Thesis
Submitted to the Graduate Faculty
of the
North Dakota State University
of Agriculture and Applied Science

By

Yaping Chi

In Partial Fulfillment of the Requirements
for the Degree of
MASTER OF SCIENCE

Major Department:
Civil Engineering

May 2012

Fargo, North Dakota

North Dakota State University
Graduate School

CHARACTERIZATION OF SURFACE MICROTOPOGRAPHY AND

DETERMINATION OF HYDROTOPOGRAPHIC PROPERTIES

By

Yaping Chi

The Supervisory Committee certifies that this ***disquisition*** complies with North Dakota State University's regulations and meets the accepted standards for the degree of

MASTER OF SCIENCE

SUPERVISORY COMMITTEE:

Xuefeng Chu
Chair

G. Padmanabhan

Zhulu Lin

Dean D. Steele

Approved:

5/14/2012
Date

Eakalak Khan
Department Chair

ABSTRACT

Spatial characterization of surface microtopography is important in understanding the overland flow generation and the spatial distribution of surface runoff. In this study, fractal parameters (i.e., fractal dimension *D* and crossover length *l*) and three hydrotopographic parameters, random roughness (RR) index, maximum depression storage (MDS), and the number of connected areas (NCA), have been applied to characterize the spatial complexity of microtopography. Clear and meaningful relationships have been established between these parameters. The RR was calculated as the standard deviation of the processed elevation, and the fractal parameters were calculated with the semivariogram method. The puddle delineation program was applied in this study to spatially delineate soil surface and to accurately determine MDS and NCA. It has been found that fractal parameters can better characterize surface microtopography. More importantly, fractal and anisotropic analyses can help to better understand the overland flow generation process.

ACKNOWLEDGMENTS

First of all, I would like to thank my advisor, Dr. Xuefeng Chu, for encouraging me to explore my interests and for providing me with a very high level of support during my study. I was particularly impressed by his enthusiasm and his open mind to new suggestions. I am also grateful for the valuable time and support from three other committee members, Dr. Zhulu Lin, Dr. G. Padmanabhan, and Dr. Dean Steele. Their critical reviews helped me to improve my thesis writing.

My research group provides me with a good learning environment. I want to give my sincere thanks to my group members, Dr. Jianli Zhang, Daniel Bogart, Jun Yang, Leif Sande, Yang Liu, Noah Habtezion, and Yingjie Yang, and my friends in the department of Civil Engineering. In addition, thanks also go to the National Science Foundation for funding this study under Grant No. EAR-0907588.

I am especially grateful to my husband and my colleague, Jun Yang, for all of his patience and support. I could not have a better partner with whom to do my research. Jun's endless love and encouragement have helped me to get through the tough times, and his continual drive for excellence and passion for his academic discipline have inspired me in my own efforts.

Last but not least, my sincere gratitude to my parents. Their love and support have made me to be ever striving for success.

TABLE OF CONTENTS

LIST OF TABLES

LIST OF FIGURES

LIST OF ABBREVIATIONS

a.....Anisotropy index

CAs .....Connected areas

D.....Fractal dimension

d_B.....Breakpoint distance

DEM.....Digital elevation model

h.....Lag distance

I_c.....Ordinate intercept

l .....Crossover length

LD .....Limiting difference

LS.....Limiting slope

MDS.....Maximum depression storage

MIF .....Microrelief index and peak frequency

MUD .....Mean upslope depression

NCA .....Number of connected areas

PD .....Puddle delineation

RR .....Random roughness

R^2.....Coefficient of determination

$\gamma(h)$.....Semivariance

S.....Local slope (%)

SD .....Standard deviation

T .....Tortuosity

CHAPTER 1. INTRODUCTION

Surface microtopography plays an important part in overland flow generation and the spatial distribution of surface runoff. Therefore, it is necessary to spatially characterize surface microtopography. Various methods and parameters have been applied to characterize surface topography. In this study, the spatial complexity of microtopography was characterized by the fractal parameters (i.e., fractal dimension *D* and crossover length *l*) and hydrotopographic parameters, such as random roughness (RR) index, maximum depression storage (MDS), and the number of connected areas (NCA). It has been found that there exist clear and meaningful relationships between these parameters to quantify surface microtopography from hydrologic point of view. The RR index was calculated as the standard deviation of the processed elevation data, and the fractal parameters were calculated using the semivariogram method. The MDS and NCA are determined using the puddle delineation (PD) program, which was applied in this study to spatially characterizing surface microtopography. Surface anisotropy was analyzed by directional semivariogram method and a modified index (*a*), which helps to better understand the overland flow generation process.

1.1 The Effect of Microtopography on Overland Flow Generation

Soil surfaces generally exhibit spatial irregularity. The complexity of surface topography relates to the spatial pattern of surface roughness, which is one of the intrinsic properties of the surface. This property has a significant influence on the behavior of the hydrologic and geomorphologic systems (Western et al. 2001), such as overland flow generation, infiltration, and sediment transport processes. Soil surface microtopography affects hydrologic processes due to the existence of topographic features such as mounds, ridges, channels, and depressions. Among those topographic features, depressions affect surface runoff by retaining a certain

amount of water during the rainfall-runoff process (Huang and Bradford 1990; Hairsine et al. 1992; Hansen 2000; Kamphorst et al. 2000; Kamphorst and Duval 2001; Darboux and Huang 2003, 2005; Abedini et al. 2006). Thus, surface depressions delay the initiation of surface runoff (Darboux and Huang 2005). It has been observed that runoff could occur even prior to the full filling of the MDS of a surface (Moore and Larson 1979; Hairsine et al. 1992; Darboux et al. 2001). MDS is determined as the maximum amount of water that can be retained in depressions on a surface. Onstad (1984) also found that more excess rainfall than the MDS is necessary in order to fill all the depressions. However, the effect of depression storage on runoff reduction decreases gradually as rainfall progresses (Onstad 1984; Helming et al. 1998). In addition, depressions affect the spatial distributions of water on a soil surface by storing water, and thus dominate the overall connectivity of the topographic surface and break the surface into a number of well connected areas (CAs) that have independent and localized hydrologic mass balance (Hayashi et al. 2003). Each localized CA consists of a depression and its contributing area. Thus, the number of CAs (NCA) can represent the complexity of surface microtopography. A higher NCA indicates stronger irregularity in surface topography (i.e., more depressions /puddles). Thus, the NCA can be used to help understand overland flow process on rough surfaces.

The spatial distribution of overland flow is greatly affected by surface microtopography, e.g., spatial variation of roughness (Zhang and Cundy 1989; Helming et al. 1998, Darboux et al. 2001). From a hydrologic point of view, surface roughness can be related to hydraulic roughness (Hairsine et al. 1992; Helming et al. 1998) that resists water flow on the soil surface and affects the velocity of overland flow (Govers et al. 2000; Darboux and Huang 2005). Helming et al. (1998) studied the effects of surface roughness and slope on surface runoff generation by conducting nine laboratory experiments with three surface characteristics (i.e., rough, medium,

and smooth) at three slopes (i.e., 17%, 8%, and 2%). Each experiment was subjected to four successive rainfall events with decreasing rainfall intensities. They found that during the first two rainfall events, flow was more apt to flow in pathways between clods on the rough surface, while surface runoff was quite uniformly distributed on the smooth surface. However, as rainfall progresses, the smooth surface also showed concentrated flow. As to the total surface runoff amount, surface roughness had a minor effect (Helming et al. 1998). In addition, they found that at the beginning of rainfall event, runoff was delayed significantly on rougher soil surface, but this topographic effect decreased as rainfall accumulates. Similarly, Moore and Singer (1990) concluded that surfaces with greater roughness led to greater infiltration rate, but this effect weakened due to the surface sealing as rainfall continued. Jester et al. (2001) examined the effects of soil microtopography and rainfall intensity on surface runoff by comparing three soil surfaces with different roughness conditions in the laboratory under various rainfall intensities. They found that the smoother surface generates higher runoff rate at the beginning of the rainfall event, and the steady-state runoff rate can be achieved earlier.

Thus, characterization of surface microtopography is important in understanding the overland flow generation and the spatial distribution of surface runoff. Furthermore, surface characterization can be helpful to analyze the hydrologic processes and conduct hydrologic modeling on rough surfaces.

1.2 Characterization of Microtopography

Digital elevation models (DEMs) are commonly used to quantify surface topography. The variation of elevations in a soil surface is often expressed in terms of surface roughness (Hairsine et al. 1992; Govers et al. 2000). Römkens and Wang (1986) categorized soil surface roughness into four types: (1) microtopography variation due to particle size (0 to 2 mm); (2)

random roughness due to cloddiness (around 100 mm); (3) oriented roughness that is mainly caused by tillage (up to 200 mm); and (4) higher order roughness at a larger scale. Similarly, Helming et al. (1998) illustrated that soil surface roughness can range from 1 mm to 100 mm on cultivated soil surfaces, which is primarily caused by secondary tillage. Over the past several decades, various techniques have been developed to obtain DEM data and quantify surface roughness for laboratory or field soil surfaces. At the early stage, a contact profile meter was used for this purpose (Kuipers 1957; Allmaras et al. 1966; Currence and Lovely 1970; Mitchell and Jones 1976; Moore and Larson 1979; Podmore and Huggins 1981). Since the late 1980s, automated non-contact microrelief meters have been developed (e.g., Römkens and Wang 1986; Huang et al. 1988). Later on, the instantaneous-profile laser scanner that can obtain high-resolution DEMs has been developed and widely used (Huang et al. 1988; Huang and Bradford 1990, 1992; Darboux and Huang 2003). This type of instantaneous-profile laser scanner has been used in the current study to acquire high-resolution DEMs of soil surface microtopography, and the random roughness of soil surfaces was studied.

With high resolution DEMs, a variety of index methods have been developed to further quantify surface roughness, such as random roughness (RR) index (Allmaras et al. 1966), tortuosity (T) (Kamphorst et al. 2000), microrelief index and peak frequency (MIF) (Römkens and Wang 1986), limiting slope (LS) and limiting difference (LD) (Linden and Van Doren 1986), mean upslope depression (MUD) (Hansen et al. 1999), and fractal dimension (Bertuzzi et al. 1990). The effectiveness of these indices in quantifying surface roughness was tested (Bertuzzi et al. 1990; Hansen et al. 1999; Kamphorst et al. 2000), and different conclusions were reached. Kamphorst et al. (2000) suggested that based on their study the RR index is highly correlated with MDS compared with other methods. Darboux et al. (2002) found that the RR index

proposed by Allmaras et al. (1966) was able to characterize soil surface roughness if the system is larger than 1 m^2. Since the RR values of various tilled soil surfaces can be easily obtained (Toy and Foster 1998), the RR index is the most widely used method (Govers et al. 2000) to quantify surface roughness. The one proposed by Allmaras et al. (1966) has been considered the standard procedure to calculate RR (Zobeck and Onstad 1987). Therefore, the RR index method was selected in this study as one of the methods to quantify soil surface roughness.

1.2.1 Random roughness method

Allmaras et al. (1966) proposed four-step procedure to calculate RR index based on the tillage surfaces. The DEM data were discretized into a number of rows (*i*) and columns (*j*). First, the logarithm of the DEM data was used so that the transformed data would exhibit a normal distribution using

$$Z'_{i,j} = Ln(Z_{i,j}) \quad (1)$$

where $Z_{i,j}$ = original elevation at row *i* and column *j*; and $Z'_{i,j}$ = logarithmic elevation at row *i* and column *j*. Then the slope and oriented tillage effects were removed using the equations

$$Z''_{i,j} = Z'_{i,j} - (\overline{Z'_i} - \overline{Z'}) \quad (2)$$

$$Z'''_{i,j} = Z''_{i,j} - (\overline{Z''_j} - \overline{Z''}) \quad (3)$$

where $Z''_{i,j}$ = elevation at row *i* and column *j* after slope removal; $\overline{Z'_i}$ = averaged logarithmic elevations at each row *i*; $\overline{Z'}$ = averaged logarithmic elevations for the entire surface; $Z'''_{i,j}$ = elevation at row *i* and column *j* after tillage removal; $\overline{Z''_j}$ = mean value of elevations (after slope removal) at each column *j*; and $\overline{Z''}$ = mean value of elevations (after slope removal) for the entire surface. Afterwards, the processed elevation data were sorted so that the upper 10% and lower 10%

of the data were removed. Finally, the RR index was calculated as the standard deviation of the processed data multiplied by the mean value of the original elevations.

$$RR = \sqrt{\frac{1}{N-1}\sum_{i=1}^{N_i}\sum_{j=1}^{N_j}\left(Z'''_{i,j} - \overline{Z'''}\right)^2} \times \overline{Z} \quad (4)$$

where N_i = number of rows; N_j = number of columns; N = total number of grids (all data points); $\overline{Z'''}$ = mean value of elevations (after tillage removal) for the entire surface; and $\overline{Z}$ = mean value of the original elevations for the entire surface. However, it is unclear why the mean value of the original elevations for the entire surface was multiplied to calculate the RR value. One possible reason is that it might be used to transfer the RR value back to represent the original surface roughness because the processed DEM data were logarithmically transformed.

Currence and Lovely (1970) provided five different ways to calculate RR index and compared their performance. They suggested that for different research or application purposes (e.g., include or exclude tillage marks), different roughness indices should be selected. For example, by calculating a plane of the best fit, the overall slope of the surface could be removed, and the RR index was calculated as the standard deviation of the residuals of the elevation. This RR index method took into consideration of the tillage effect. However, both slope and tillage effects can be removed by correcting elevations for each row and column of a DEM, and the resulting RR value represents surface roughness without slope and tillage effects (Currence and Lovely 1970). Planchon et al. (2001) argued that Allmaras et al. (1966) did not provide enough detailed information on how to remove tillage effects. Thus Planchon et al. (2001) developed another method to calculate RR index as the standard deviation of elevations after removing the slope and tillage effects. Overall, it has been well accepted that the rougher the surface is, the higher the RR value.

Usually a rough surface can store a certain amount of water in depressions. The relationship between roughness indices and MDS of a rough surface has been examined by a considerable amount of research. To derive this relationship, MDS is often expressed as the maximum equivalent water depth that can be stored on a rough soil surface (Govers et al. 2000). Since the 1980s, various regression equations have been suggested to estimate MDS based on surface roughness indices, such as RR index (Onstad 1984; Mwendera and Feyen 1992), LD and LS (Linden et al. 1988), and MUD (Hansen et al. 1999). The performances of these indices for quantifying soil surface roughness, estimating MDS, and describing surface changes from rainfall-induced soil erosion have been examined and evaluated (Bertuzzi et al. 1990; Huang and Bradford 1992; Hansen et al. 1999; Govers et al. 2000; Kamphorst et al. 2000). Among these indices, RR index has been proven to be the one that has the highest correlation with MDS (Kamphorst et al. 2000).

As to the RR index-based method, MDS is also a function of slope besides the RR index (Onstad 1984; Mwendera and Feyen 1992). Thus, slope is another important factor in estimating MDS. Onstad (1984) proposed a regression equation relating MDS with RR and slope based on microrelief data from over 1000 plots with slopes ranging from 2% to 12%. Similarly, Mwendera and Feyen (1992) studied MDS based on surfaces with slopes from 1% to 15%. Hansen et al. (1999) further extended slopes up to 20% for MDS estimation. It has been found that surfaces with higher RR values have larger depression storage values for the same slope (Onstad 1984; Mwendera and Feyen 1992). Given a rough surface at various slopes, a milder slope retains more water in depressions than a steeper slope does (Onstad 1984; Huang and Bradford 1990; Hairsine et al. 1992; Mwendera and Feyen 1992). Thus, in this study, the slope effect was taken into consideration when calculating the RR and MDS values.

The past studies to calculate RR index for soil surfaces were mostly carried out on the tillage surfaces. However, according to Chu et al. (2012), for the random roughness surfaces without tillage marks, a modified RR calculation method provides better estimation of RR and MDS values to quantify soil surface roughness at mild slopes. This method was modified from Allmaras et al. (1966), but only included removing the slope effect of the DEMs and the upper and lower 10% of the data before calculating RR index, while the other two steps (i.e., logarithmic transformation of the data and tillage removal) were not involved (Chu et al. 2012). In this study, surfaces without tillage marks were selected to analyze surface microtopography; thus, the RR calculation method provided by Chu et al. (2012) was employed.

1.2.2 Fractal method

Huang and Bradford (1992) suggested that RR index was inadequate to describe surface roughness because this single index was efficient to capture the variance in vertical elevations but unable to describe the spatial correlation of the soil surface. Two surfaces with the same RR value may exhibit completely different surface characteristics (Huang 1998). Therefore, Huang and Bradford (1992) proposed a combination of fractal and Markov-Gaussian model to represent complex surface roughness.

Fractal analysis has been widely used to characterize the spatial complexity of soil surfaces (Mark and Aronson 1984; Klinkenberg and Goodchild 1992; Quattrochi et al. 1997; Huang 1998; Vázquez et al. 2005, 2007). The typical characteristic of fractal is being self-similar. Objects can be self-similar in the following different ways: being self-similar (i.e., identical at all scales), being quasi self-similar (i.e., exhibits the same pattern at different scales), being statistical self-similar (stochastically repeats a pattern), and being qualitatively self-similar (i.e., in a time series) (Falconer 2003). Theoretically, a surface can be considered as statistically self-

similar when enlargements of any subsets of the surface have a statistical distribution identical to that of the whole surface (Feder 1988). In practice, self-similarity can be determined by evaluating the linearity of the best-fit curve of semivariance [$\gamma(h)$] and lag distance (h) on the log-log plot of $\gamma(h)$ vs. h during the calculation of fractal dimension (D) using the semivariogram method (Yokoya et al. 1989; Klinkenberg and Goodchild 1992). If the curve is approximately linear for all lags, the surface is consistent with the concept of self-similarity (Mark and Aronson 1984), and mono-fractal analysis can be applied. In reality, however, such a surface rarely exists. Most surfaces may be partially self-similar, so a fractal model can be applied only within a limited range or distance (Mark and Aronson 1984; Yokaya et al. 1989; Xia 1993; Huang 1998; Vázquez et al. 2007; Abedini and Shaghaghian 2009). Out of the range, different D values may exist for the surfaces (Mark and Aronson 1984). Thus, many studies have been conducted to examine the multifractal property of surface topography, which involved identification of breakpoints and determination of multiple linear segments and the corresponding D values (e.g., Mark and Aronson 1984; Klinkenberg 1988; Lovejoy et al. 1995; Gagnon et al. 2006; Abedini and Shaghaghian 2009). Mark and Aronson (1984) found that most of their selected geographic surfaces showed varying D values at different scales. D values derived from the middle scale were always greater than those from the smaller scale.

One of the major fractal parameters is D. Generally, D ranges from 2 to 3 for a topographic surface (Mark and Aronson 1984; Roy et al. 1987; Huang and Bradford 1992; Sun et al. 2006). A surface with fractal D can be considered as its capability to "fill" the space in which it resides (Abedini and Shaghaghian, 2009). Thus, the more a surface fills the space, the higher D it has (Sun et al., 2006). Therefore, surfaces with high D values appear more disordered or display a rapid succession of peaks and valleys in a short distance, but show slow variability at a

large distance (Sung et al. 1998). On the contrary, surfaces with low *D* values have greater variations in elevation (e.g., large and deep depressions), and thus more space is left "unfilled." Based on the fractal analysis of some agricultural soil surfaces, Huang (1998) concluded that a relatively lower *D* value of a surface indicated higher contrast of aggregates/clods on the surface, while a higher *D* value denoted overall gradual/minor changes in surface elevations. It has been observed that a surface with *D* value greater than 2.5 implies a negative spatial autocorrelation between two points at the scale where *D* is derived (Burrough 1983; McClean and Evans 2000), so detailed topographic information may be lost at a sampling interval larger than that scale. In contrast, surfaces with *D* values smaller than 2.5 are less rugged and show positive spatial autocorrelation within the scale associated with *D* (Burrough 1983). Thus, elevations can be interpolated from their neighboring points without losing too much information for this type of surface (Mark and Aronson, 1984).

Different methods have been used to calculate *D*. Xia and Clarke (1997) summarized seven methods, among which three widely used methods are the semivariogram method, the box-counting method, and the walking dividers method. The reliability of the three methods in calculating *D* value has been evaluated, and the semivariogram method has been widely accepted to calculate *D* (Klinkenberg and Goodchild 1992; Xia 1993). A semivariogram is the plot of $\gamma(h)$ as a function of *h* along the specified direction, since *h* is a separation vector that has both magnitude and direction. Therefore, the semivariogram technique is a geostatistical method that can describe the change of spatial continuity with the distance and direction (Isaaka and Srivastava, 1989). When applying semivariogram to characterize surface topography, it represents the variations in elevations as the distances between two data points increase along certain direction. Usually, as the separation between two points increases, the $\gamma(h)$ value at the

corresponding distance (h) generally increases, which indicates that there exists correlation between those points. However, this increase in variance gradually slows down and finally reaches a plateau or quasi-plateau at certain distance (Isaaka and Srivastava, 1989), indicating no correlation between two points exists beyond that distance. Due to the spatial distribution of data, the semivariogam curve may show some dips, which are often expressed as "Hole effect" (Isaaka and Srivastava, 1989). This "Hole effect" suggests that two points separated further away show more similar features than those at shorter distance. This phenomenon exists in the datasets where natural cyclicity occurs (Isaaka and Srivastava, 1989), such as the cycles of sedimentary faces change and the reoccurrences of depressions on surfaces. It has been verified that semivariogram was able to characterize the spatial patterns of the soil surface (Linden and Van Doren 1986; Helming et al. 1993). One of the major advantages of the semivariogram method for fractal analysis is that it can quantify not only overall (i.e., omnidirectional) variability of surface topography, but also the directional variability (i.e., anisotropy) (Xia 1993; Vázquez et al. 2005). One property of the semivariogram is that the $\gamma(h)$ values calculated along any two opposite directions are identical (Isaaka and Srivastava, 1989), resulting in the symmetric distribution of $\gamma(h)$ about the origin. For an omnidirectional semivariogram, at each distance h, all pairs that fall into that distance along any direction are included for calculating $\gamma(h)$. However, this does not mean that along all directions, the spatial continuity is the same (Isaaka and Srivastava, 1989). The anisotropy of surface topography suggests that the variability of the surface is different along various directions. This anisotropy can be captured by the directional semivariogram method. Along any specific direction, $\gamma(h)$ values can be calculated at the corresponding h. Vázquez et al. (2005) applied the semivariogram method to capture the tillage direction of agricultural fields since the D value is much higher along the tillage direction.

Klinkenberg (1988) calculated angular variograms to quantify surface anisotropy and detect the dominant directions of surface roughness.

In the application of the semivariogram method for fractal analysis, however, it is critical to determine the breakpoint distances (d_B) to find the best-fit linear regression lines of the semivariogram curve at different scales in the calculation of *D*. The d_B is the maximum distance, at which the best regression line can be fitted (Xia and Clarke 1997; Sung et al. 1998). In other words, the d_B is a "boundary" scale, within which a single *D* can be applied for the corresponding linear segment. Thus, within the distance of two neighboring breakpoints, it can be considered as a homogeneous region unit (Pentland 1984; Abedini and Shaghaghian 2009). However, the only limitation of applying the semivariogram method in fractal analysis is that the determination of d_B to find the best-fitting curve is a quite subjective procedure, which is the sole determining factor of the *D* calculation. A controversial problem may exist in determining which segment of the semivariogram is linear. McClean and Evans (2000) found that the least-square regression method yielded a smaller slope for the log-log semivariogram, resulting in a higher *D* value. Especially when no perfect linear scatters exist, the least-square method can be biased due to the denser points for longer distance lags (McClean and Evans 2000). Thus, McClean and Evans (2000) fitted the linear curve by visual decision that any points starting from the curved transition sections should be excluded from the linear part. In other words, the d_B for linear part is determined when any point starts to deviate from the linear line (McClean and Evans, 2000). Their method is similar to that of Mark and Aronson (1984) and Pentland (1984), who also fitted the best linear line by visual estimation. According to Klinkenberg and Goodchild (1992), when using the least-square method to fit the best linear segment of the semivariogram, a d_B is generally selected so that the scatter of points was not too curved, and that the coefficient of

determination R^2 is greater than 0.9. Until now, there is no common criterion on how to determine the d_B.

D may not be a unique parameter for characterizing surface topography. Two surfaces of dissimilar topographic features may have the same *D* value (Klinkenberg 1988; Huang and Bradford 1992). Together with *D*, the ordinate intercept (I_c) of the best-fit linear segment of the semivariogram also has been used to characterize surface topography (Klinkenberg and Goodchild 1992; Abdini and Shaghaghian 2009). Alternatively, crossover length (l), which is derived from I_c, is often combined with *D* to characterize soil surface microrelief (Huang and Bradford 1992; Vázquez et al. 2005, 2007). *D* represents the horizontal variability in surface roughness with scale while I_c or l reveals the degree of vertical topographic variations at a reference scale (Klinkenberg 1988; Klinkenberg and Goodchild 1992; Huang and Bradford 1992; Vázquez et al. 2007). "In other words, *D* is an index for the proportional distribution of different-sized elements in a relative scale, and l is the scaling parameter transforming the relative size to actual scale."(Huang and Bradford 1992). For the same scale, a rougher surface has a greater l value (Eltz and Norton 1997). Huang and Bradford (1992) observed that l is more sensitive than *D* to represent soil roughness changes.

In applications of the semivariogram method, any data trend (e.g., slope) should be removed to satisfy the major assumption introduced in this method (Perfect and Kay 1995). Because the sample semivariogram can estimate its theoretical semivariogram only when the sampling data are stationary, which implies that the sampling data have zero expected value (SAS Institute Inc. 2009). However, Armstrong (1986) found that removal of periodic components had no substantial effect on the computation of semivariance, and hence the *D* value. Abdini and Shaghaghian (2009) also found that surface detrending methods (e.g., linear,

quadratic, and cubic fitting plane methods) had a minimal effect on *D*. Armstrong (1986) and Klinkenberg and Goodchinld (1992) suggested that for fractal analysis of surfaces topography, it is not necessary to remove the non-stationarity of the data in the semivariance calculation since surface slope is a part of the topographic properties. However, Vázquez et al. (2010) removed the slope of soil surface microrelief by finding a best fitting plane (linear, quadratic or cubic fitting plane), and concluded that trend removal did affect the fractal indices (*D* and *l*). Thus, further studies are needed to evaluate the effect of surface trend removal on fractal analysis.

1.3 Objectives

Now that the fractal parameters (*D* and *l*), RR, MDS, and NCA all can be used to characterize surface microtopography, it should be of importance to examine their relationships, which will further improve our understanding of the effect of surface microtopography on overland flow processes. However, both the random roughness method and the fractal method quantify microtopography statistically, regardless of the spatial distribution of surface characteristics, such as the location and size/depth of the depressions, which are critical in controlling the overland flow initiation. Thus, spatially delineating surface depressions and determining their properties are necessary to understand the mechanism of surface runoff and help develop more physically based hydrologic models. The objectives of this study are to (1) characterize surface microtopography by fractal analysis and three hydrotopographic parameters (RR, MDS, and NCA) and examine the relationships of these hydrotopographic parameters with the fractal parameters *D* and *l*; (2) evaluate the effect of surface slope removal on fractal analysis; (3) analyze the anisotropic properties of surfaces by using the directional semivariogram method and a modified anisotropic index to identify the dominant roughness direction; (4) investigate the possibility to use the fractal parameter *D* and *l*, and the anisotropy analysis results to improve the

understanding of the overland flow generation process; and (5) spatially delineate topographic surfaces to accurately determine hydrotopographic properties (i.e., MDS and NCA) of a soil surface.

CHAPTER 2. STATISTICAL CHARACTERIZATION OF SURFACE TOPOGRAPHY

This chapter focuses on surface microtopography characterization using statistical methods, e.g., random roughness method and fractal method. First, the procedures of how to calculate RR index and fractal parameters (*D* and *l*) are detailed. Then applications of these methods in analyzing surface microtopography are performed. Eight surfaces that were created in the laboratory and field were selected for this purpose. The RR index was used to quantify overall variation of a DEM. The fractal method was applied to characterize surface spatial properties at different scales as well as the vertical variation in elevations. The anisotropic property of surfaces was also investigated using the fractal method. The fractal *D*, *l*, and the anisotropy results were analyzed to improve the understanding of overland flow generation. In addition, two more hydrotopographic parameters (MDS and NCA) have been determined from the puddle delineation (PD) program (Chu et al. 2010). The detailed information on how to calculate MDS and NCA are described in Chapter 3. Efforts have been made to examine the relationships of fractal *D* and *l* with RR, MDS, NCA.

2.1 Calculation of Random Roughness (RR) Index

Two procedures are implemented to process the DEM data in the application of the random roughness method (Allmaras et al. 1966) in this study. First, the overall slope of a surface is removed:

$$Z''_{i,j} = Z_{i,j} - (\bar{Z}_i - \bar{Z}) \tag{5}$$

The processed elevation data are then sorted to remove the upper 10% and lower 10% extreme data points. Finally, the RR of a surface can be expressed as standard deviation (*SD*) of the processed elevation data:

$$RR = SD = \sqrt{\frac{1}{N-1}\sum_{i=1}^{N_i}\sum_{j=1}^{N_j}\left(Z''_{i,j} - \overline{Z''}\right)^2} \tag{6}$$

2.2 Calculation of Fractal Parameters (*D* and *l*)

As mentioned previously, the semivariogram method was used to calculate fractal parameters in this study. Based on the DEM data, semivariance is given by:

$$\gamma(h) = \frac{1}{2N(h)}\sum_{i=1}^{N(h)}[Z(s_i + h) - Z(\mathbf{s}_i)]^2 \tag{7}$$

where $\gamma(h)$ = semivariance; s_i = location *i*; *h* = lag distance has both magnitude and direction; $Z(s_i)$ = elevation at location s_i; $Z(s_i + h)$ = elevation at location $(s_i + h)$; and $N(h)$ = number of pairs spaced at *h*.

Based on the calculated semivariance $\gamma(h)$, *D* and intercept (I_c) can be determined. For a fractal Brownian motion (fBm) model, the elevation change $\Delta Z(h)$ and the structural function are respectively given by (Huang and Bradford 1992):

$$\Delta Z(h) \propto h^H \qquad (0 < H < 1) \tag{8}$$

and

$$\gamma(h) \propto h^{2H} \tag{9}$$

where *H* = Hurst exponent; and $\Delta Z(h)$ = difference in elevations at distance *h*. Thus, the semivariance $\gamma(h)$ can be expressed as:

$$\gamma(h) = Kh^{2H} \tag{10}$$

or

$$\log[\gamma(h)] = 2H\log(h) + \log(K) \tag{11}$$

where K = proportionality factor. Eq. (11) shows a linear relationship between log [$\gamma(h)$] and log (h) with a slope (S) of $2H$ and I_c of log(K). That is, $H = S/2$. Given the Hurst exponent H, the fractal dimension D of a topographic surface (Euclidean dimension $d = 3$) is given by:

$$D = 3 - H = 3 - 0.5S \tag{12}$$

Following Huang and Bradford (1992), K in Eq. (10) can be expressed as a function of crossover length l, and Eq. (10) can be rewritten as:

$$\gamma(h) = l^{2-2H} h^{2H} \tag{13}$$

Thus, l can be determined by K and H from the best-fit linear line of the semivariogram in the log-log plot. Here, the term "crossover length" is used because based on Eq. (13), it is a special length that when $l = h$, $\gamma(h) = l^2$. Fig. 2.1 schematically shows the procedure for determining D, I_c, and d_B by using the semivariogram method.

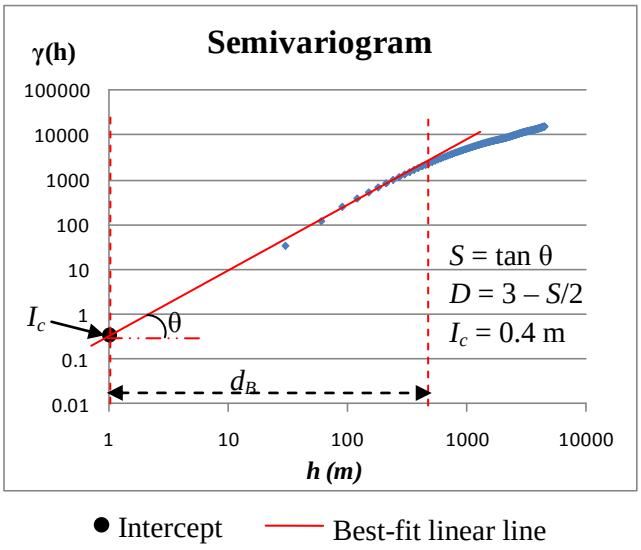

Fig. 2.1 Determination of fractal dimension D, ordinate intercept I_c, and breakpoint distance d_B

As mentioned previously, the key step to calculate D is to find the best-fit linear segment of the semivariogram curve; but it is inappropriate to determine the d_B based on R^2 only. Personal judgment based on the real condition is another important factor. Firstly, on the log-log plot of

the semivariogram, the turning points will be identified by visual decision, and the first linear segment of the semivariogram curve can be fitted by the least-square regression method. The higher the R^2 value, the better the linear line is fitted to the curve. Secondly, adjustment can be performed to make sure that points starting from the curved transition section should be excluded from the linear part. In addition, the fitted linear line must be close to the first few points of the semivariogram curve, because the first linear segment captures the detailed surface characteristics, and two points at closer distance show more detailed spatial information of a surface than those further away. If this condition has not been satisfied, go back to the first step, exclude the points around the curved transition section, and then fit the linear segment again so that the fitting line can be close to the first few points. In this way, the first d_B can be determined. For some surfaces, more linear lines can be fitted starting from the curved section. Thus, multiple linear lines can be fitted to the corresponding linear segments, if applicable, to analyze the fractal properties of the surfaces at different scales. The fitting point of the second linear segment starts from the point next to the last point of the first fitted curve. The d_B for the second or third linear segment can be determined based on the same criteria as those of for the first linear segment. The goodness of fit of the least-square regression can be evaluated by:

$$R^2 = 1 - \frac{\sum_{i=1}^{n} (\gamma_i - \hat{\gamma}_i)^2}{\sum_{i=1}^{n} (\gamma_i - \bar{\gamma})^2} \tag{14}$$

where R^2 = coefficient of determination; γ_i = actual semivariance at i^{th} distance; $\hat{\gamma}_i$ = estimated semivariance at i^{th} distance; $\bar{\gamma}$ = average value of the actual semivariance for all distances; and n = total number of lag distances h for semivariance calculation.

A Windows-based fractal analysis program has been developed in this study by using C# (Microsoft 2005) to facilitate the computation of omnidirectional and directional semivariance $\gamma(h)$, D, and I_c. This program was developed to calculate fractal parameters (i.e., D and l) in addition to semivariogram. The main Windows interface includes a map area and a control panel, which are used for importing DEM data, inputting the parameters for semivariance calculation, computing the semivariance, plotting the semivariogram in either a normal plot or a log-log plot, and fitting the first linear segment of the semivariogram curve for the computation of D and I_c (Fig. 2.2). The angles are described as follows: 0 ºis defined as east and angles proceed in a counter-clockwise direction where 90 ºis north, 180 ºis west and 360 ºreturns to the east direction. Using the fractal analysis program, directional semivariance for any angles ranging from 0 ºto 360 ºcan be calculated. The input parameters include the number of lags, lag distance (h), lag tolerance, angle, angle tolerance, and bandwidth (Fig. 2.2). An omnidirectional semivariance can be calculated by setting the angle tolerance greater than or equal to 90 º. The outputs include the semivariance, semivariogam, the number of pairs for the corresponding lag distance, and D and I_c from the first linear segment of the semivariogram.

In order to verify the accuracy of the fractal analysis program in calculating the semivariance, the semivariance from this program was compared with that from the GSLIB software package (Deutsh and Journel 1998). A series of surfaces with various topographic characteristics were selected for this purpose. Specifically, both omnidirectional and directional semivariance (along any directions) were computed by using both software packages and the results were evaluated. Fig. 2.3 shows the comparison of the semivariogram calculated by the fractal analysis program and GSLIB for omni direction, x direction (0 º), and 75 ºdirection. The semivariograms from the two software packages match perfectly for all three directions,

indicating that the fractal analysis program is accurate in calculating the semivariance, and the resultant fractal parameters are valid.

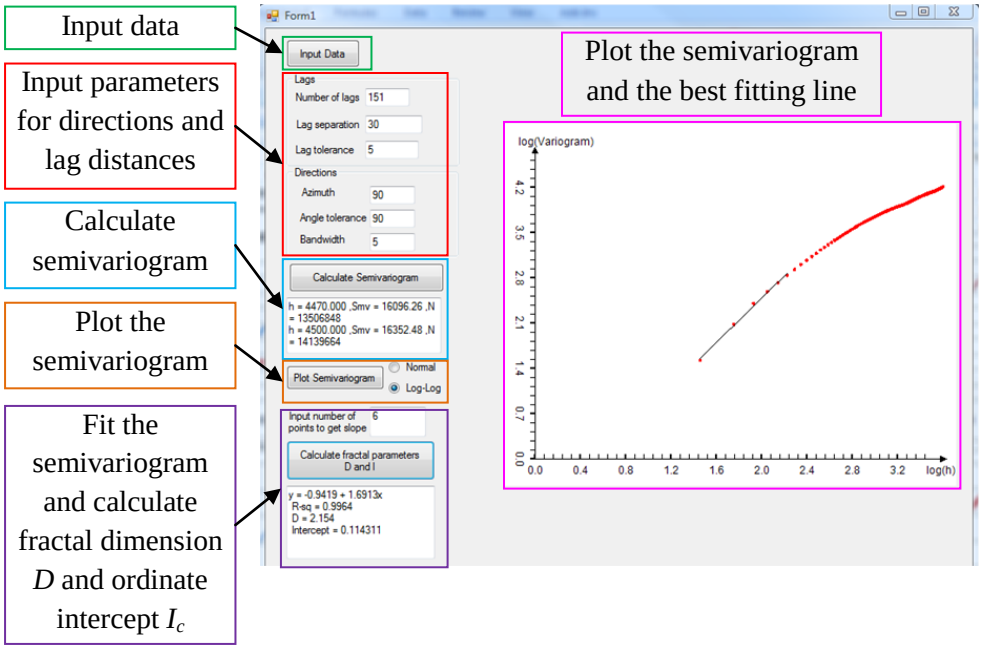

Fig. 2.2 Windows interface of the fractal analysis software

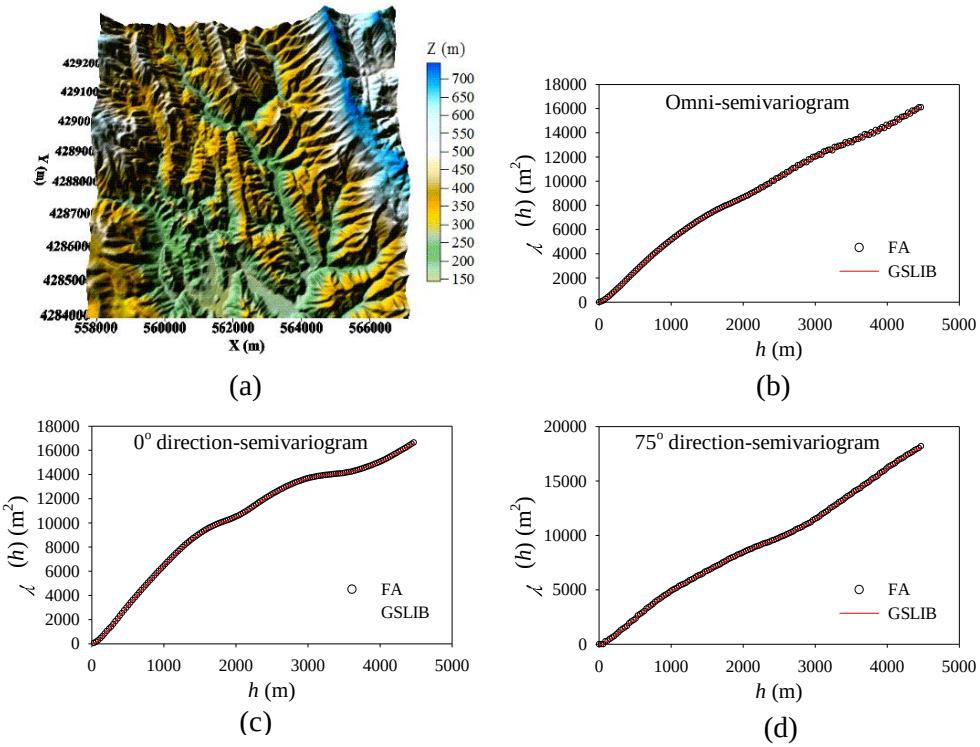

Fig. 2.3 Comparison of semivariograms calculated by the fractal analysis program and GSLIB for omni-direction, 0 °direction, and 75 °direction

2.3 Surface Data

Six laboratory-scale soil surfaces (S1 – S6) and two field plot surfaces (S7 – S8) were created (Fig. 2.4). Surfaces S1 – S6 (Figs. 2.4a – 2.4f) were created in the lab by randomly distributing the soil aggregates across the area (i.e., no oriented roughness). The sizes of major aggregates increase gradually from S1 to S6. Those aggregates were collected in the field that is to the west of North Dakota State University campus without any vegetation. Since these aggregates were used to create surface topography, the texture of the soil has not been tested. The aggregates were broken down to small ones to create the surface with small aggregates (e.g., S1 and S2). The area of S1 – S6 was 0.6 m $\times$ 2.0 m. The two field plot surfaces of an area of 6.0 m $\times$ 3.2 m, S7 and S8 (Figs. 2.4g and 2.4h), respectively represented rough and smooth field surfaces. The rough surface (i.e., S7) was created with mounds and depressions using hand tools, and the smooth surface (i.e., S8) that was characterized without any obvious depressions was also created by hand tools. Both two surfaces were graded to a 2.5% slope. The laboratory and field surfaces were scanned by using an instantaneous-profile laser scanner (Darboux and Huang 2003). The scanned data were then processed and high resolution digital elevation model (DEM) data were generated. The roughness of the eight surfaces were quantified using the RR method, and the MDS and NCA of each surface were calculated by the PD program. Surface S8 was used for evaluating the effect of slope removal on the computation of semivariance and consequently D and l. The anisotropy of the surfaces (S1 – S8) was analyzed to identify the dominant roughness directions. Moreover, Surfaces S1 – S6 were utilized to examine the relationships between D and RR, MDS, and NCA, which were further used to interpret how surface microtopography might affect the overland flow process on rough surfaces.

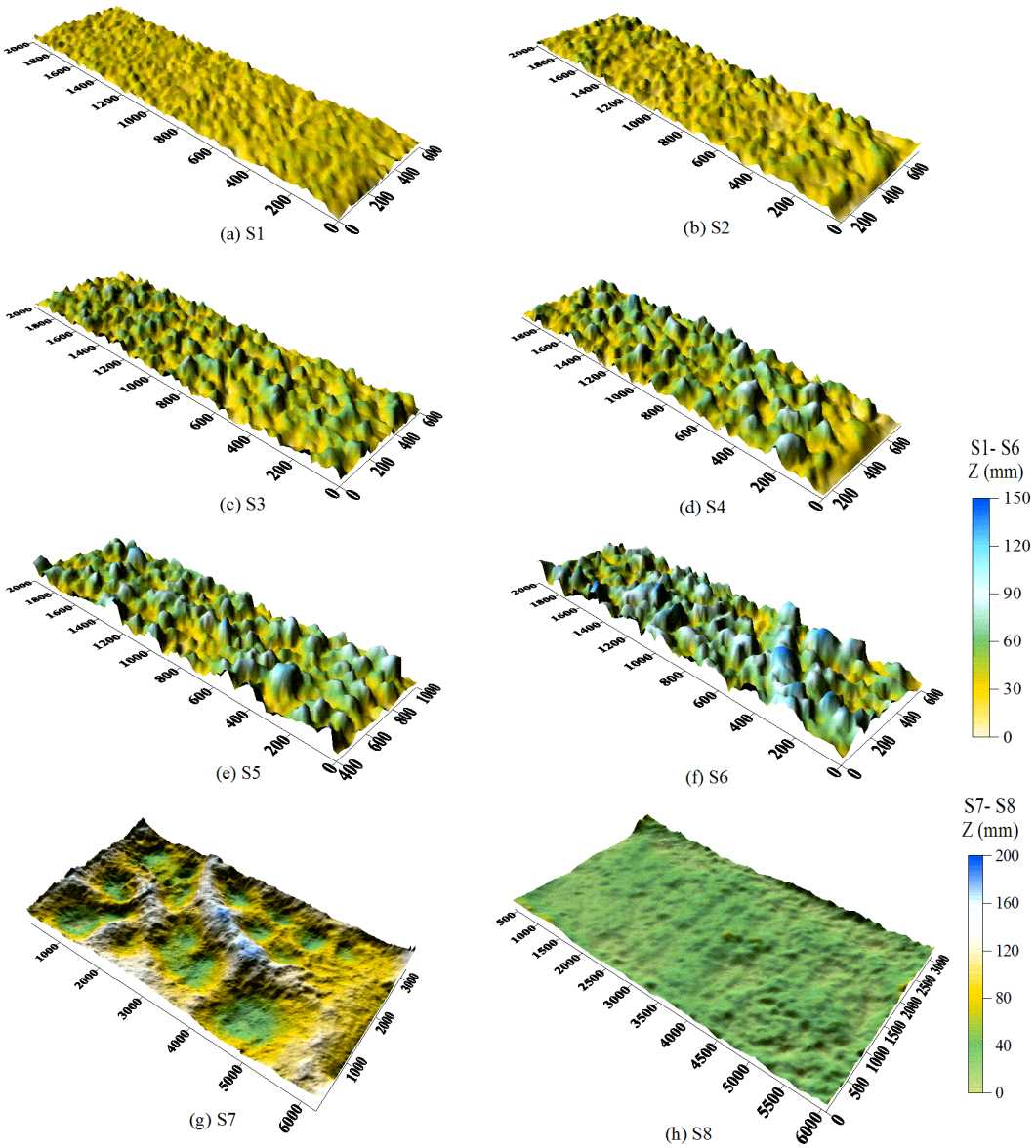

Fig. 2.4 Six laboratory surfaces (S1 – S6) and two field surfaces (S7 – S8)

2.4 Anisotropy of Surface Microtopography

Anisotropy was analyzed for the eight surfaces (Fig. 2.4) by calculating *D* values along different directions. Anisotropy of the surface microtopography is defined when the *D* values of a surface vary among those directions, while isotropy refers to the situation where *D* values along any direction are identical. In this study, besides omnidirectional semivariograms, directional semivariograms were calculated for angles from 0 ºto 360 ºwith an interval of 15 ºfor

these surfaces. D and l were then determined for all directions and plotted in rose plots to show their directional distributions. In addition, an anisotropy index (a) was calculated to further quantify the anisotropic/isotropic properties of surface topography. This index was originally proposed by Green and Erskine (2004):

$$a = 10^{\Delta D} \tag{15}$$

where $\Delta D = D_{max} - D_{min}$. This anisotropy index is "a ratio of the standard deviation between measurements in orthogonal directions" (Green and Erskine 2004). However, this ΔD only captures the maximum difference in D values by comparing them in two directions. To account for the anisotropy of surface topography, the variation along all directions should be considered. Therefore, a modified calculation of a index is proposed in this study:

$$a = 10^{SD(D)} \tag{16}$$

where $SD(D)$ = standard deviation of D along all the directions (i.e., 24 directions in this study). Theoretically, a equals 1 for a perfectly isotropic surface (i.e., $SD(D) = 0$), and increases with the degree of anisotropy.

2.5 Effect of Surface Slope Removal

Surface S8 was used to evaluate the effects of surface slope on the calculation of fractal parameters (D and l). The surface slope was removed by finding a best-fit plane (linear, quadratic, or cubic fitting plane) based on the highest R^2 value. Then, the effect of surface detrending on fractal analysis was evaluated by comparing the fractal parameters (including D and l) of the surfaces with and without slope removal.

2.6 Determination of MDS and CAs

Based on the DEM of each surface, the PD program was utilized to identify puddles and their relationships, determine flow directions and flow accumulations, and compute the MDS of

the surface. Flow directions are determined based on the D8 method (O'Callaghan and Mark 1984) that water flows from one cell along the steepest downward slope by comparing the eight neighboring grid cells, in either orthogonal or diagonal directions. In addition, the CAs and NCA were determined through a searching process in the PD program, which identified all hydrologically connected cells. The detailed information of how to calculate MDS and NCA is provided in Chapter 3.

In this study, we first investigated the general relationships between *D* and RR, MDS, and CA for Surfaces S1 – S6. Then, efforts were made to link these parameters to the overland flow generation processes.

2.7 Applications of the RR Index for Characterizing Surface Microtopography

For the six laboratory surfaces, the RR values increase from 0.44 cm to 1.50 cm, and the MDS values increase from 1370.16 cm^3 to 3207.74 cm^3 as soil aggregates become larger from S1 to S6 (Table 2.1). Note that the MDS values are calculated using the PD program that will be described in the following chapter. It can be inferred that the RR values can capture the overall roughness of the surface topography with a higher RR value representing greater contrast of surface elevations (e.g., S6) and a lower RR value indicating much milder variability in elevations (e.g., S1). RR and MDS have a direct relationship. Surfaces with a low RR value (e.g., S1) are usually characterized with shallow or small depressions, resulting in a low MDS; while the rougher surface with greater aggregates (e.g., S6) are dominated by the puddles that are deeper or bigger, leading to a high MDS. This conclusion is consistent with the findings by Chu et al. (2012) that overall, MDS has a positive relationship with RR.

As to the two field surfaces S7 and S8 (Figs. 2.4g and 2.4h), the resultant RR values are 1.90 cm and 0.46 cm, and the MDS values are 2.20×10^5 cm^3 and 2.47×10^4 cm^3, respectively.

The significant difference in the RR values for these two surfaces suggests dissimilar surface topography. Surface S7 is dominanted by depressions across the entire surface while S8 is relatively smooth with no obvious puddles on the surface (Figs. 2.4g and 2.4h). Similarly, the much greater MDS of S7 also indicates much rougher surface topography than that of S8.

Table 2.1. Random roughness (RR) and the maximum depression storage (MDS) for the six laboratory surfaces (S1 – S6)

Surfaces	S1	S2	S3	S4	S5	S6
RR (cm)	0.44	0.62	0.89	1.12	1.29	1.50
MDS (cm^3)	1370.16	1690.43	1863.61	2058.57	2512.35	3207.74

However, the RR index cannot interpret the spatial correlation of surface topography, and it does not provide the scale information of the surface. For example, S1 and S8 have similar RR values (RR = 0.44 cm for S1 and 0.46 cm for S8), but these two surfaces are at different scales and appear totally dissimilar. That is, S1 is a laborary surface with an area of 1.2 m^2, while S8 is a field surface with an area of 19.2 m^2. In addition, these two surfaces show distinct surface features (Figs. 2.4a and 2.4h). Huang (1998) also addressed this issue that a surface may appear to have high random roughness at one scale but may exhibit some pattern at other scales. Again, S6 and S7 have similar problems. With a RR value of 1.50 cm, S6 is characterized with quite randomly distributed large aggregates (Fig. 2.4f), while S7 with a RR value of 1.90 cm is featured by spatially distributed puddles (Fig. 2.4g). Thus, the RR index may be inadequate to spatially describe complex topographic surfaces. Consequently, the RR index based MDS calculation method may not be able to provide accurate estimation of the real depression storage on a surface, which has been demonstrated by Chu et al. (2012).

2.8 Application of Fractal Analysis on Surface Microtopography

2.8.1 Surface detrending effect on fractal analysis

The field surface S8 (Fig. 2.4h) was selected for evaluating the surface detrending effect on fractal analysis. For S8, the best-fit plane is a cubic one (R^2 = 0.999). Fig. 2.5 shows the comparison of omnidirectional semivariograms of the surfaces with and without surface detrending. It can be observed that surface slope significantly affects the computation of semivariance (Fig. 2.5). For a sloping surface without slope removal, the semivariance increases continuously with increasing *h* due to the overall slope-related increase in elevations. After slope removal, the semivariance reaches a sill beyond a distance of about 700 mm (Fig. 2.6h). Although the semivariograms may be similar within a short distance with and without slope removal, they change significantly for a larger *h* after surface slope removal or detrending (Fig. 2.5). The differences in the distributions of semivariogram imply that significant changes in fractal parameters *D* and *l* are expected. Accordingly, the scale (i.e., d_B) at which *D* is determined varies. Table 2.2 shows the *D*, *l*, and d_B values calculated for surfaces with and without detrending or slope removal. It can be observed that the *D* and *l* values are 2.50 and 0.15 mm at the scale of 320.12 mm with detrending, while they are 2.43 and 0.08 mm at the scale of 1,340.74 mm without detrending. As the scale (i.e., d_B), at which *D* and *l* were derived, changes beyond 1,000 mm, the relative difference in *D* is 2.88% while the relative difference in *l* reaches up to 87.50%, inidcating that *l* is more sensitive to the slope removal. The larger d_B value without slope removal indicates that two points further away (i.e., up to the distance of the d_B = 1340.74) might show certain correlation, which is due to the overall slope in this example. However, with slope detrending, two points beyond the distance of 320.12 mm are not related.

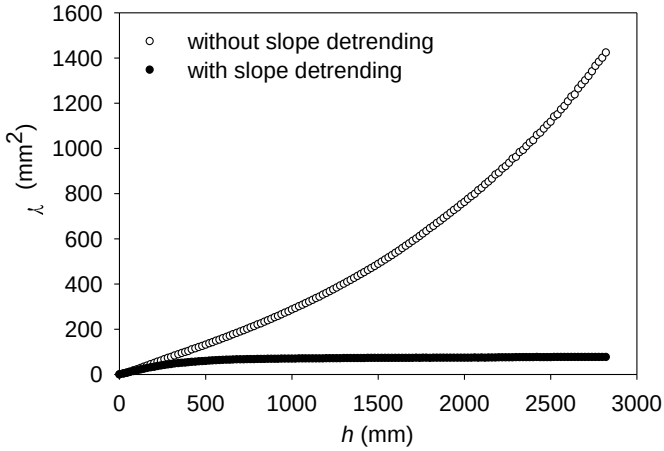

Fig. 2.5 Comparison of omnidirectional semivariograms for S8 with and without surface detrending

Table 2.2. Fractal dimension (D), crossover length (l), and breakpoint distance (d_B) values for S8 with and without surface trend removal

	D	l (mm)	Breakpoint distance (d_B) (mm)
Without Detrending	2.43	0.08	1340.74
With Detrending	2.50	0.15	320.12
Relative difference (%)	2.88	87.50	76.12

The preceding discussion demonstrates that surface slope removal significantly changes the semivariogram, and consequently affects the fractal parameters D and l. Though slope is one of the major attributes of surface topography, it will disturb the quantification of surface roughness. Therefore, surface slope should be removed before calculating semivariance and applying fractal analyses to characterize surface microtopography. In this study, the overall slope for each surface was removed before analyzing surface microtopography. However, slope effect should be considered during the analyses of topography related processes, such as surface runoff process, sedimentation process, and solute transportation process.

2.8.2 Monofractal and multifractal analysis of surface topography

Figue 2.6 shows the omnidirectional semivariograms for the six laboratory surfaces (S1 – S6) and the two field surfaces (S7 – S8). All the eight semivariograms reach a plateau or sill at certain distances, which vary among surfaces (Fig. 2.6). The distance at which the semivariogram reaches sill is defined as the range. Both sills and ranges increase from S1 to S6 as the size of soil aggregates becomes larger (Figs. 2.6a – 2.6f). For S1 – S6, the semivariances increase rapidly for small lag distances (h), which indicates a close correlation for small scale elevation variations. The increasing rate of a semivariogram implies how quick the influence of a sample drops off with distance. Then, the semivariance becomes relatively stable (sill) beyond a certain h, which varies slightly among surfaces (Figs. 2.6a – 2.6f).

For both field plot surfaces S7 and S8 (Figs. 2.4g and 2.4h), the semivariance values increase significantly within small lag distances (h) and then approach to their sill values (Figs. 2.6g and 2.6h). However, the variance value (sill value) for S7 reaches up to about 1,200 mm^2 and the sill value of S8 is only approximately 70 mm^2, which indicates that S7 exhibits much greater variations in elevations than S8 does. The semivariogram of S8 show an asymptotic sill beyond the lag distance (h) of around 700 mm, implying that beyond this lag distance no spatial correlation exists. Oscillation in surface microtopography of S7 can be observed for the larger h part of the semivariogram curve of S7 (h is greater than 1,300 mm) (Fig. 2.6g). In addition, slight differences in the semivariograms at the short distance between S7 and S8 can be observed that a region of low slope near the zero distance occurs in S7 (Fig. 2.7g). This is because for S7, the data those within short distance vary smoothly. For example, the puddle surface is smooth (Fig. 2.4g). However, S8 is overall smooth but show small variations in elevation at small distance (Fig. 2.4h), resulting in more rapid increase in the semivariance value.

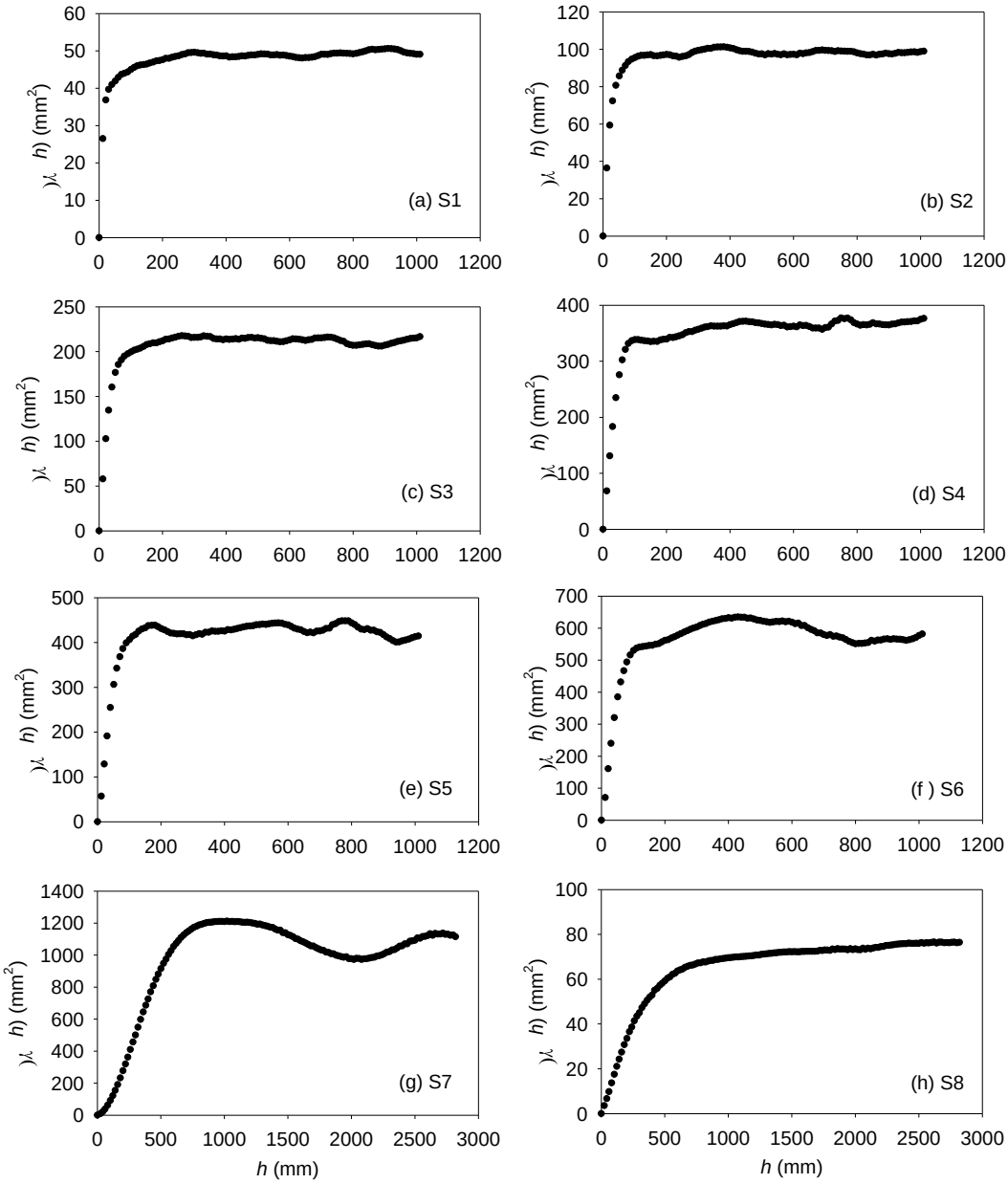

Fig. 2.6 Omnidirectional semivariogram for the six laboratory surfaces (S1 – S6) and two field surfaces (S7 – S8)

Fig. 2.7 shows the omnidirectional semivariograms for the eight surfaces (S1 – S8) in log-log plots with the fitted linear red lines that are used to derive the *D* and *l*. It can be seen that only one linear segment is observed for the semivariograms of the six random rough surfaces (S1 – S6) within certain distances, thus fractal analysis focuses on one linear segment for these six surfaces (Figs. 2.7a – 2.7f). For the two field plot surfaces (S7 and S8), however, the

semivariograms exhibit two distinct linear segments before reaching the sills (Figs. 2.7g and 2.7h). Thus, multifractal analysis is performed for these two surfaces by fitting two linear segments on the semivariogram curves. The first linear segment characterizes the smaller scale surface topography, while the second segment reveals larger scale topographic variability.

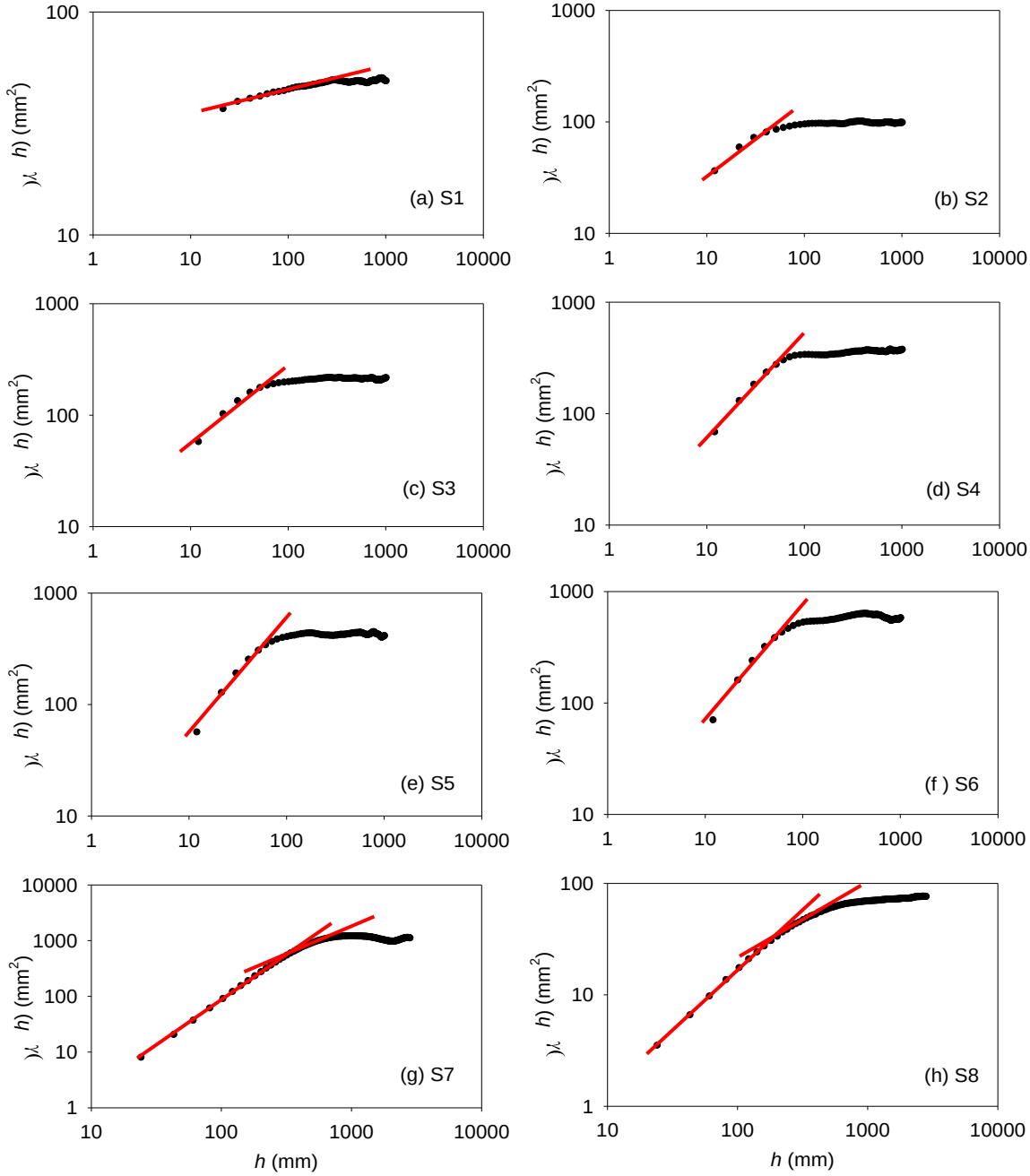

Fig. 2.7 Omnidirectional semivariogram for the six laboratory surfaces (S1 – S6) and two field surfaces (S7 – S8) in log-log plot

Table 2.3 shows the results of omnidirectional fractal parameters for S1 – S6. *D* values decrease gradually as soil aggregates become larger (Table 2.3). S1 with the smallest soil aggregates shows rapid changes in mounds and depressions on the surface, indicating more irregularity and thus resulting in a higher *D* value. This result is consistent with the findings by Zribi et al. (2000) and Sun et al. (2006). In contrast, S6 with the largest soil aggregates has the lowest *D* value since the change of elevations is more gradual and smoother at local scales. The *D* values for the six surfaces (S1 – S6) decrease from 2.95 to 2.65. The *l* values vary from 5.86 mm for S1 to 11.30 mm for S6 (Table 2.3). However, surfaces with dissimilar topographic characteristics may have similar *D* values. For example, the difference in *D* values between S2 and S3 is small (0.05), but their difference in *l* values is as high as 2.59 mm (Table 2.3). This is due to the distribution of aggregates on both surfaces. S2 and S3 both are characterized with randomly distributed soil aggregates, but the average clod size of S3 is greater that of S2 (Figs. 2.4b and 2.4c). A similar *D* value suggests that the proportions of aggregate size distribution are similar for both surfaces, while a higher *l* value indicates greater variability in surface elevations at the actual scale. Thus, a rougher soil surface (i.e., with bigger size of clods) has a higher *l* value. Hence, *D* and *l* should be jointly used to quantify surface topographic properties.

Table 2.3. Omnidirectional fractal dimension (*D*), and crossover length (*l*) for the six laboratory surfaces (S1 – S6)

Surfaces	S1	S2	S3	S4	S5	S6
D	2.95	2.89	2.84	2.72	2.69	2.65
l (mm)	5.86	7.46	10.05	10.31	10.31	11.3

Table 2.4 shows the omnidirectional fractal parameters for S7 and S8 at the two scales. S7 has much smaller *D* and *l* values for the small scale (D = 2.20, l = 0.0005 mm, and d_B = 419.89 mm) than those for the large scale (D = 2.63, l = 1.97 mm, and d_B = 700.77 mm) (Table

2.4). This low *D* value of S7 at the small scale captures the characteristics of local depressions and mounds on the surface. Because the sizes of major depressions on S7 are about 400 – 500 mm in diameter (Fig. 2.4g), and the scale at which *D* and *l* are derived is within this range (i.e., d_B = 419.89 mm). Note that a *D* value close to 2 implies that less volume of the surface is "filled"; while a high *D* value close to 3 suggests that the surface is almost "filled" to reach the 3D dimension. This conclusion can be verified based on the microtopographic characteristics of S7. Within the scale of the depressions (i.e., *h* = 400 – 500 m), more space is "unfilled", and the vertical variation of elevations is small, resulting in low *D* and *l* values. In addition, a low *D* value indicates that the surface is "smooth" at the corresponding scale. The elevation points within this scale are correlated so that the elevation of any point can be interpolated by its neighboring points. However, beyond this scale, the detailed information of the surface is missing, resulting in a sharp change in the semivariogram curve. This break at the horizontal scale leads to the fractal *D* changes. Elevations may change significantly at a larger scale (a larger *h*) (Sung et al. 1998). In this study, *D* and *l* from the secondary segment reveal large scale topographic features, such as the distribution of depressions across the entire surface. *D* and *l* values from the second segment are much greater than those for the first segment (Table 2.4), implying that at a larger spatial scale (*h* = 419.89 – 700.77 mm) more significant changes in elevations dominate the surface topography for Surface S7.

Table 2.4. Omnidirectional fractal parameters for two field surfaces (S7 – S8) at two scales

Surfaces	Segments	Fractal Dimension (*D*)	Crossover Length (*l*) (mm)	Breakpoint Distance (d_B) (mm)
S7	1st segment	2.20	0.0005	419.89
	2nd segment	2.63	1.97	700.77
S8	1st segment	2.50	0.15	320.12
	2nd segment	2.79	1.65	680.10

Similar results can be observed for S8. That is, *D* and *l* values from the secondary segment are higher than those of the first segment (Table 2.4). The *D* value of 2.79 at the scale of 320.12 - 680.10 mm indicates that the auto covariance of surface elevations at this scale is low. In other words, the surface is relatively disordered. In spite of the overall smoothness of S8, small variations in surface elevations are random (Fig. 2.4h). Overall, S8 has greater *D* values than S7 for both segments, indicating much more rapid local changes in surface elevations for S8 (Table 2.4). Based on *D* and *l* values, it can be concluded that at a small scale S7 shows significant topographic variations with spatial scales along the horizontal direction (low *D*), and smaller vertical variability in elevations (low *l*) at the reference scale. S8 looks smooth (high *D*), but the local variability in elevations is greater (higher *l*). Thus, multifractal analysis can be a useful way to identify the scale, at which the dominant topographic characteristics of surfaces change. This critical scale is determined based on the obvious change in the semivariogram curve and the calculated *D* value. Thereafter, the d_B (i.e., critical scale) should be another important parameter in fractal analysis in that the variation of *D* and *l* for any surface is dependent on the d_B value.

2.8.3 Analysis of anisotropic properties of surface topography

Anisotropy of microtopography was analyzed for the eight laboratory and field surfaces by using directional fractal parameters. Fig. 2.8 shows the rose plots of *D* and *l* for S1 – S6 along the 24 selected directions. The circular shape of the *D* and *l* curves indicates the isotropic property of those surfaces; while the noncircular curves represent the anisotropic property of topographic surfaces. As has been mentioned previously, the $\gamma(h)$ values calculated along any two opposite directions are identical (Isaaka and Srivastava, 1989). Therefore, the derived *D* and

l values are symmetrical about the origin, which can be observed from Fig. 2.8. Accordingly, the following discussions of anisotropy analyses will focus on the upper portion (0 º– 180 º).

For S1 – S6, soil aggregates are randomly distributed, and there are no slope and oriented tillage marks (Figs. 2.4a – 2.4f). Since it has been verified that *D* and *l* should be jointly used to analyze surface topography in Section 2.8.2, *D* and *l* are examined side by side to study the surface anisotropy. The variation of *D* and *l* values along different directions indicates that these surfaces are not uniform, and exhibit anisotropy. However, only minor directional variations in *D* and *l* can be observed for all the six microtopographic soil surfaces (Fig. 2.8). Particularly, S1 with the smallest aggregates show quite uniform distributions of *D* and *l* values, indicating that S1 is close to isotropy (Fig. 2.8). As soil aggregates become larger, the variations of *D* and *l* are more significant from S1 to S6, which means that S6 shows more obvious anisotropy (Fig. 2.8). Generally, *D* decreases and *l* increases from S1 to S6 as the sizes of aggregates increase (Fig. 2.8). These decreasing or increasing patterns are consistent with the results from the omnidirectional fractal parameters.

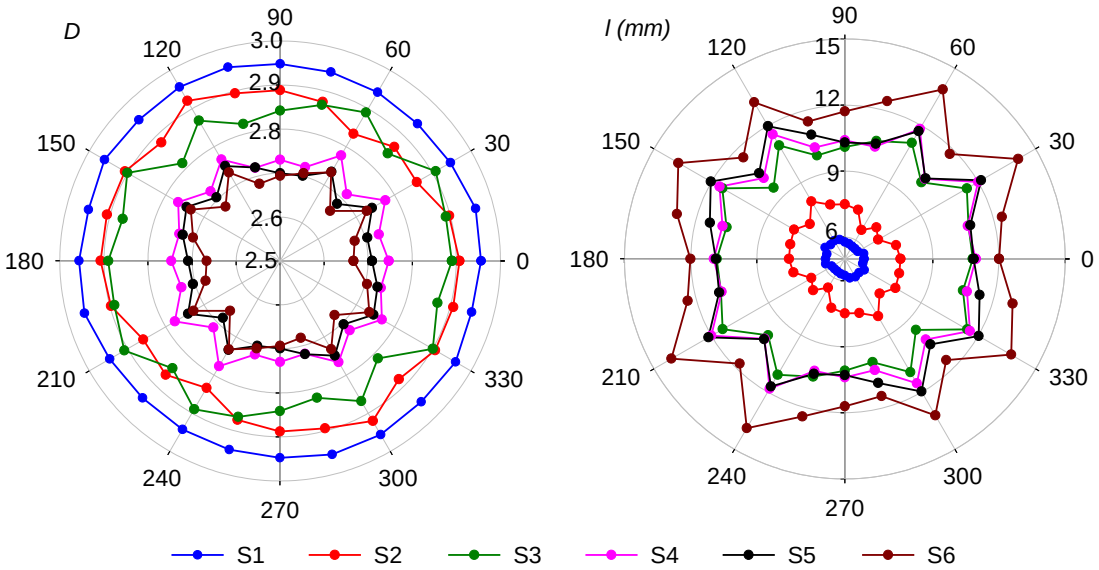

Fig. 2.8 Distributions of fractal dimension *D* and crossover length *l* for S1 – S6 along the 24 selected directions

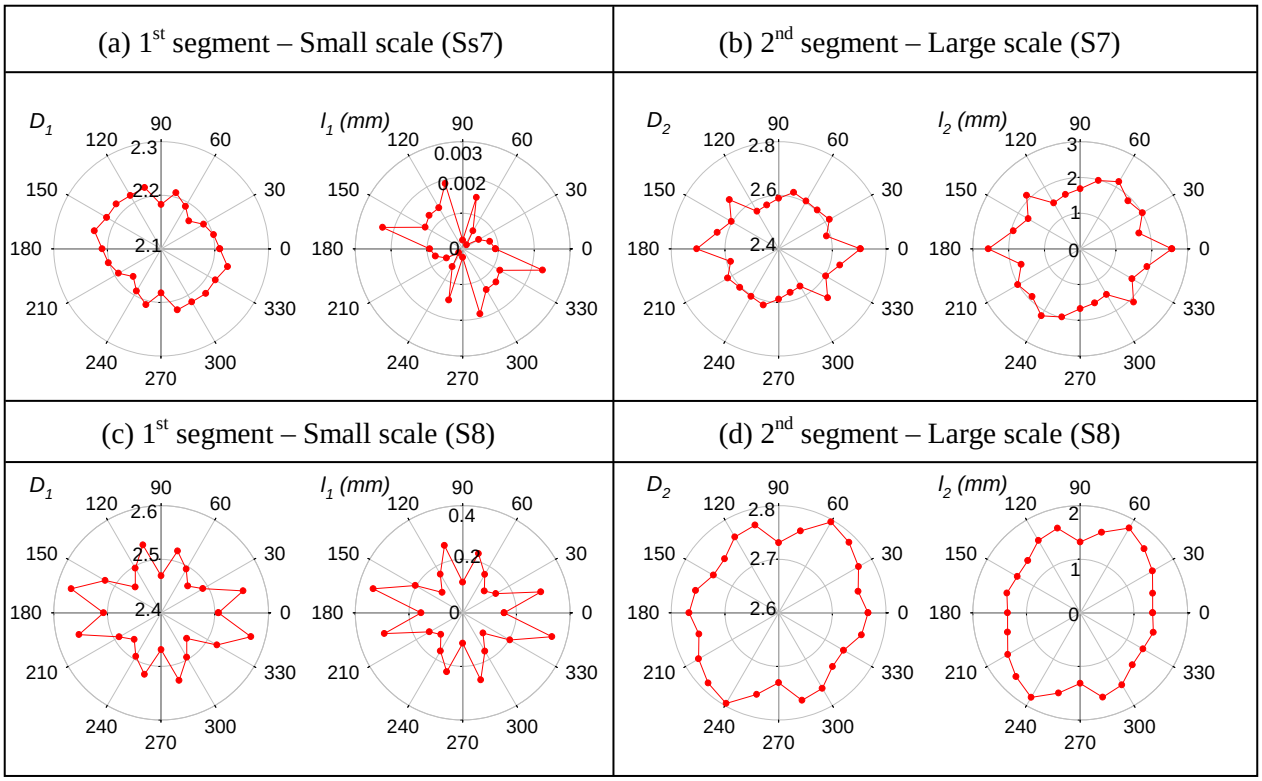

Fig. 2.9 Distributions of fractal dimension *D* and crossover length *l* for S7 – S8 along the 24 selected directions at two scales

Fig. 2.9 shows the distributions of fractal *D* and *l* for the two field surfaces S7 and S8 along the 24 selected directions at two scales. For S7 at the small scale (first segment), *D* captures the detailed topographic information within the local depression scale of the surface. The *D* values range from 2.17 (along 45 °) to 2.23 (along 165 °) with small variation, which shows slight anisotropy (Fig. 2.9a). This is because the shapes of the depressions on S7 do not have any directionally distributed patterns (Fig. 2.4g). However, *l* values of S7, ranging from 0.0002 mm to over 0.002 mm (Fig. 2.9a), exhibit obvious anisotropic properties. The *l* values depict the vertical elevation changes along different directions. Even though the change in *l* seems great, the changing magnitude actually is of an order of 10^{-3} (Fig. 2.9a). Thus, the vertical variation in surface elevations at the small scale is small. On the contrary, the *D* values of S7 at the large scale (second segment) show more anisotropic properties. The *D* values along 90 °–

120 °are the smallest among all directions (Fig. 2.9b). This can be attributed to the surface microtopography of S7. Along 90 °– 120 °, surface microtopography exhibits more undulation because of the two major ridges across the surface, but the change in elevations is smooth and gradual (Fig. 2.4g).

For S8, *D* and *l* show stronger anisotropic distributions at the small scale and more isotropic distributions at the larger scale, which are opposite from S7 (Figs. 2.9c and 2.9d). For this relatively smooth surface S8, the changes in elevation at the small scale represent the local variations associated with small aggregates. At the larger scale, the correlation between elevation points is low and the surface looks smooth. Thus, the surface had relatively uniform distributions of *D* and *l* along all directions (Fig. 2.9d).

It should be noted that S7 shows more anisotropy at larger scale than S8 does at smaller scale (Fig. 2.9). This difference can be attributed to their distinct topographic features. The overall distribution of depressions across S7 can be captured by the anisotropically distributed *D* and *l* at the large scale, while the topographic information of each depression can be depicted at the small scale. For S8, the characteristic of overall smoothness can be captured by the distributions of *D* and *l* at the larger scale, while the minor variations in elevations at the small scale across the surface result in the non-uniform distributions of *D* and *l* (Fig. 2.9). Thus, the directional fractal parameters *D* and *l* can be useful indicators for quantifying the anisotropic properties of topographic surfaces.

Table 2.5 shows the calculated anisotropy index (*a*) values [Eq. (16)] for the eight surfaces. Though the rose plots of S1 – S6 show the variations of *D* and *l* along different directions (Fig. 2.8), the variations are quite uniform, resulting in small *SD*(*D*). Therefore, the *a* value that is dependent on *SD*(*D*) is small. Basically, the *a* values for the six laboratory surfaces

(S1 – S6) are very close except for S1 (Table 2.5). S1 has the lowest *a* value, indicating that the surface with small aggregates possesses highly isotropic properties. As to the field plot surfaces, S7 and S8 show stronger anisotropy with higher *a* values at the large and small scales, respectively (Table 2.5). These findings are in accordance with those from the rose plots showing the directional distributions of *D* in Figs. 2.8 and 2.9. Thus, the anisotropy index *a* can be effectively used to quantify the anisotropic property of surface microtopography.

Table 2.5. Anisotropy index (*a*) for the six laboratory-scale surfaces (S1 – S6) and the two field surfaces (S7 – S8)

Surfaces	S1	S2	S3	S4	S5	S6
Anisotropy index (*a*)	1.01	1.06	1.07	1.05	1.05	1.06
Surfaces	S7		S8			
	1st segment	2nd segment	1st segment	2nd segment		
Anisotropy index (*a*)	1.04	1.09	1.08	1.04		

2.9 Relationships between D and RR, MDS, and NCA

For S1 to S6, the *D* values decrease from 2.95 to 2.65 (Table 2.3), and the NCA values decrease from 117 to 60, except for S3 (Table 2.6). However, the RR values increase from 0.44 cm to 1.50 cm, and the MDS values increase from 1,370.16 cm^3 to 3,207.74 cm^3 from S1 to S6 as their soil aggregates become larger (Table 2.1). Fig. 2.10 shows the relationships between *D* and RR, MDS, and NCA. Generally, a random rough surface with a greater *D* value (e.g., S1) has smaller RR and MDS values, and a higher NCA value. That is, such a surface (S1) is relatively smooth (low RR), has shallow and small depressions/puddles (low MDS), and consists of many isolated areas (high NCA). However, a surface with a smaller D value (e.g., S6) has greater variations in surface elevations (high RR), deeper and larger depressions/puddles (high

MDS), and fewer isolated areas (low NCA). These dissimilar topographic characteristics of the surfaces affect their responses to a rainfall event.

Table 2.6. The number of connected areas (NCA) for the six laboratory-scale surfaces (S1 – S6)

Surfaces	S1	S2	S3	S4	S5	S6
NCA	117	92	99	89	66	60

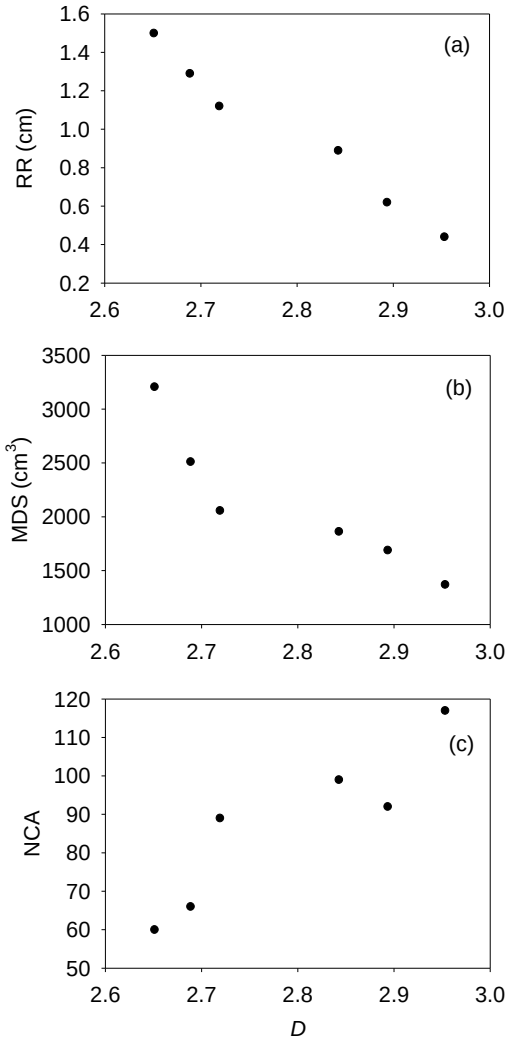

Fig. 2.10 Relationship between fractal dimension *D* and random roughness (RR), maximum depression storage (MDS), number of connected areas (NCA) for the six random roughness surfaces (S1 – S6)

In summary, a rougher soil surface of a smaller *D* value has a higher RR, which results in a greater MDS. This implies that *D* and MDS are inversely correlated. NCA depends on the

number of depressions/puddles on the surface. A complex surface that consists of more puddles has a higher *D* value. Since RR, MDS and NCA are able to characterize surface microtopography, one of the essential factors that control hydrologic processes; it is of interest to relate these hydrotopographic parameters to the fractal parameters *D* and *l* to explore the potential to apply *D* and *l* to improve the understanding of the related hydrologic processes.

2.10 Fractal Analysis in Relation to Overland Flow Processes

Fig. 2.11 shows the overland flow experiments conducted on S7 and S8. It can be observed that the distributions of water on the surfaces are controlled by their topographic conditions. At the small scale (first segment), S7 with a smaller *D* is featured with bigger and deeper puddles that are capable of storing more water (Fig. 2.11a). Within each puddle, the elevation change between two points is small at the small spatial scale (i.e., the puddle surface is locally smooth), as quantified by the smaller *l* value (Table 2.4). Thus, water transfers easily within each puddle. At this small scale, the effect of surface roughness on overland flow is minimal. In contrast, at the large scale (secondary segment), S7 is characterized with a greater *D* value and a much higher *l* value (Table 2.4), showing the overall rough surface features (e.g., distribution of puddles). At this large scale, surface topography plays an important role in the overland flow process since water movement is greatly affected or controlled by the "larger scale" puddles. Similarly, S8 with larger *D* and *l* values at the large scale (secondary segment) shows an overall higher roughness, which affects surface runoff.

S8 is characterized with smaller and shallower puddles and a greater number of small CAs than S7 (Fig. 2.11b). The difference in overland flow between these two surfaces is determined by the overall difference in their topographic conditions. S7 with a lower *D* value has the potential to retain more water in depressions of the surface, which in turn redistributes

surface runoff water, enhances infiltration in the depressions, and delays surface runoff generation. In contrast, S8 with a greater *D* value has smaller depression storage and surface runoff occurs earlier than S7 with a lower *D* value.

(a) Surface S7 with water (b) Surface S8 with water

Fig. 2.11 Pictures from field experiments to demonstrate the hydrologic processes for S7 and S8

Another important factor that controls the drainage system is the anisotropic/isotropic properties of surface microtopography. According the fractal parameters *D* and *l*, the six lab surfaces (S1 – S6) show relatively isotropic properties (Fig. 2.8). For an anisotropic surface, the dominant roughness exists along the directions of lower *D* values. For example, S7 shows anisotropy in *D* at the large scale (secondary segment) (Fig. 2.9b). The *D* values are small in the directions of 90 °– 120 °(i.e., north to northwest) (Fig. 2.9b), along which surface runoff is hindered/blocked by continuously distributed ridges (Fig. 2.11a). For other directions, more puddles can be hydrologically connected (Fig. 2.11a). For S8, its small and shallow puddles are distributed more evenly, resulting in stronger isotropy, and thus no obvious directional runoff process exists (Fig. 2.11b). Attention should be paid that the above analyses were based on surfaces with slope effects removed. Slope affects the surface runoff direction, but it is not the focus of this study.

From the above analyses, it can be concluded that the spatial complexity of the overland flow processes is highly dependent on the surface topographic conditions. The fractal parameters

D and *l* can provide useful information that helps understand the related hydrologic processes. It is of great importance to examine the mechanisms of overland flow generation and surface runoff processes under the influence of surface microtopography.

2.11 Summary

In this study, six laboratory surfaces and two field plot surfaces were created; and the random roughness (RR) index and the fractal analyses were conducted for quantifying the surface microtopography. The semivariogram method was applied for calculating the fractal parameters. A semivariogram is the plot of $\gamma(h)$ as a function of h along the specified direction. The linearity of the $\gamma(h)$ curve suggests the fractal behavior of the surface topography. By plotting the semivariogram on a log-log plot and fitting a linear line to the linear segment of the $\gamma(h)$ curve, the *D* and *l* values can be derived from the slope of this fitted line and the ordinate intercept. It has been demonstrated that RR index can capture the overall surface roughness, with higher RR value indicating rougher surface topography and lower RR value representing relatively smooth surfaces. However, the RR index cannot account for the spatical correlation of surface topography, and it does not provide scale information of the surface. Thus, two surfaces at different scales may result in the same RR value.

However, the fractal dimension *D* combined with crossover length *l* are able to quantify the spatial and vertical variance of surface topography. The fractal *D* value is scale dependent, which describes horizontal roughness, and *l* represents vertical variability in elevations at the reference scale. Particularly, anisotropy/isotropy of surface microtopography was examined for the selected surfaces by directional fractal analysis, and further was quantified by introducing a modified anisotropy index. It was found that surface slope removal had a significant effect on the calculation of fractal parameters. Since overall surface slope adds the correlation between two

upstream and downstream points, it will disturb the quantification of surface roughness. Therefore, surface slope should be removed before calculating semivariance and applying fractal analyses to characterize surface microtopography. However, being an important topographic attribute, slope effect should be considered during the analyses of topography related processes, such as surface runoff. It was demonstrated that multifractal analysis was able to capture surface topographic features at different scales. Fractal dimension *D* and crossover length *l* at smaller scales depicted more details on surface microtopography, while the overall topographic features were characterized by *D* and *l* at larger scales. This study showed that *D* was inversely correlated with random roughness RR and maximum depression storage MDS, and was directly related with the number of connected areas NCA. Since surface microtopography affects the distribution of runoff water and development of the drainage system, the parameters that are able to characterize surface topography (e.g., RR, MDS, NCA, and the fractal parameters *D* and *l*) can be effectively used to help understand the overland flow generation process. A surface with a smaller *D* value has the potential to retain more water on the surface (in depressions), which in turn redistributes surface water, enhances infiltration in the depressions, and delays surface runoff generation. The dominant surface roughness exists along the directions of smaller *D* values. Along those directions, surface runoff is prone to be hindered/blocked by continuously distributed ridges. Other directions possess better hydrologic connectivity.

CHAPTER 3. DELINEATION OF PUDDLES AND DETERMINATION OF THEIR HYDROLOGIC PROPERTIES

As has been stated in the previous chapter, fractal parameters (*D* and *l*) and the hydrotopographic parameters (RR, MDS, NCA) were able to effectively characterize surface microtopography, which is important and necessary for hydrologic modeling since more accurate surface characterization can help develop more realistic hydrologic models. However, it is difficult to accurately calculate MDS and NCA. Thus, the PD program was applied in this study to overcome this problem.

Many studies have been done in the past to calculate the maximum depression storage (MDS) of a soil surface, but those researches calculated the MDS indirectly from roughness indices, and averaged the MDS as the maximum equivalent water depth that can be stored on a surface (Onstad 1984; Mwendera and Feyen 1992; Hansen et al. 1999; Kamphorst et al. 2000). As more and more high-resolution DEM data are available these days, various methods have been developed to estimate more accurate MDS directly by using DEMs (Ullah and Dickinson 1979; Huang and Bradford 1990; Martz and Garbrecht 1993; Hansen et al. 1999; Kamphorst and Duval 2001; Planchon and Darboux 2002). Except for Planchon and Darboux (2002), other researchers implemented a similar algorithm to calculate MDS. That is, the local minima were first located based on DEM, and then the depressions were gradually filled with water until the spilling point has been reached. In this way, the MDS of a rough surface was calculated by summing the amount of water that fills all depressions on a surface. However, Planchon and Darboux (2002) described their method of first submerging the entire surface with a thick layer of water and then draining all the excess water that overflows the depressions. The remaining water on the surface is determined as the MDS.

3.1 Introduction to the Puddle Delineation (PD) Program

The Windows-based puddle delineation (PD) program (Chu et al. 2010) is one of the programs using numerical methods, developed to characterize surface microtopography, delineate puddles and their relationships, calculate MDS, and determine topographic and hydrologic properties such as slope, aspect, flow directions, flow accumulations, and contributing areas. It has been verified by Chu et al. (2010) that the PD program provides accurate MDS not only for an individual puddle/depression, but also for the entire surface. The NCA of a soil surface was determined based on the flow directions. The main Windows interface of the PD software includes a map area, the data input area, and result displaying area (Fig. 3.1). The main interface shows the summarized puddle delineation results, including the MDS of the entire surface and the contributing area for any user specified cell (Fig. 3.1). The detailed results can also be accessed in the formats of text documents and 2D figures.

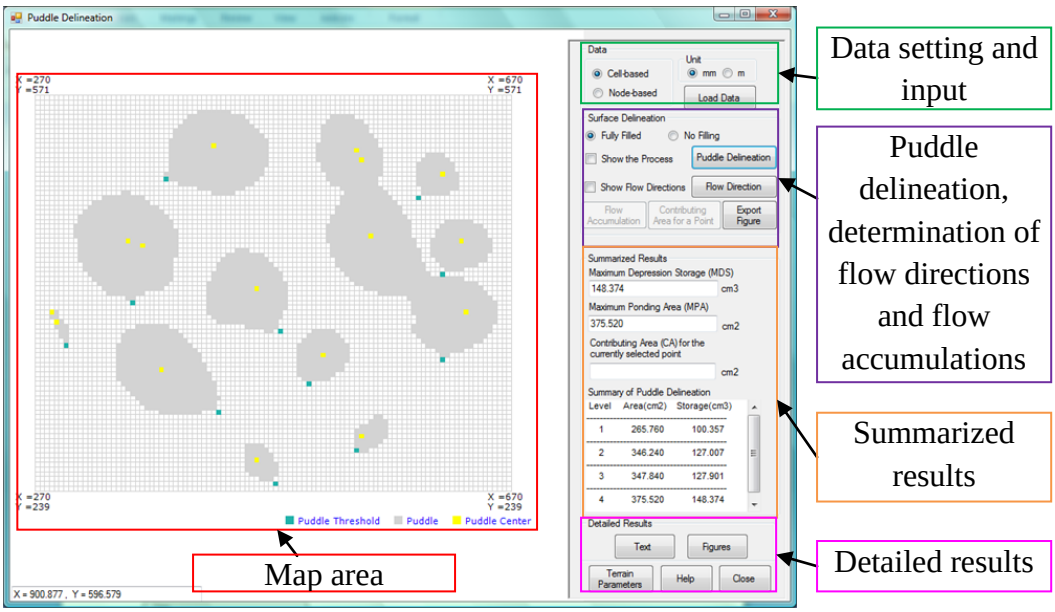

Fig. 3.1 Interface of the Windows-based Puddle Delineation Software

Prior to calculating the MDS of a surface, all puddles have to be delineated. To identify puddles with any size on a surface, the PD program first identifies the center(s) of each puddle. The center is the cell with the lowest elevation compared with the elevations of its surrounding eight cells. Then the puddle searching/expansion process starts from the identified center(s). Following a set of criteria, all cells belong to each puddle are included in the puddle. The searching process continues until threshold cell(s) has been met. The threshold cell is the one through which water in the puddle can flow out. Thus, puddles are then determined for the entire surface.

3.1.1 Determination of flow directions and contributing areas

Flow directions are determined for all cells based on the D8 method (O'Callaghan and Mark 1984). In this program, numbers 1 to 8 represent the flow directions of east, south, west, north, southeast, southwest, northwest, and northeast, respectively. For boundary cells along the entire study area, water flows out of the boundary if those boundary cells have a lower elevation than their neighboring cells. That is, an open boundary condition is assumed. For puddle centers, the concept of "no flow direction" has been introduced. That is, a zero flow direction value is given to all puddle centers. Based on flow directions, the contributing area of any specified cell can be determined. Since puddles break the connections on the surface, water accumulated in the local minima (i.e., puddles). Thus, each cell within the puddle has a unique contributing area, with the puddle centers having the largest contributing area.

3.1.2 Calculation of MDS and NCA

After all puddles have been identified, the MDS of the entire surfaces as well as for any individual puddle can be calculated. Within each puddle, the elevation difference between the threshold cell and each cell of that puddle is the maximum depth of water that cell can retain.

Then the volume of water that each cell can hold can be calculated as the maximum depth multiplied by the area of that cell. The summation of the volume of water calculated for each cell within a puddle is the MDS of that puddle. The MDS for the entire surface can be expressed as (Chu et al. 2010):

$$MDS = \sum_{i=1}^{n} \sum_{j=1}^{m_i} \left(zt_i - z_{i,j} \right) \Delta x \Delta y \tag{17}$$

where MDS = maximum depression storage of the entire surface; n = number of puddles; m_i = number of cells in puddle i; zt_i = elevation of the threshold of puddle i; $z_{i,j}$ = elevation of cell j within puddle i; Δx = size of a cell along x direction; and Δy = size of a cell along y direction. The scheme of calculating the MDS is shown in Fig. 3.2.

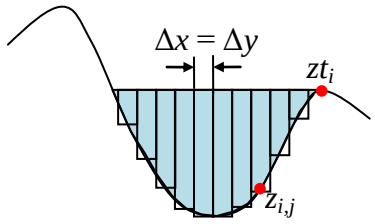

Fig. 3.2 Scheme of calculating maximum depression storage (MDS) of a puddle

Similarly, the NCA of a surface can be calculated. To determine the CAs, the puddle centers and outlet cells have to be located first, which can be obtained from the puddle delineation results and the calculated flow directions. Then, the contributing cells to each puddle center and outlet can be tracked by the flow directions. Thus, the NCA of a surface equals the number of puddles plus the number of outlets of that surface. Each CA consists of a puddle or an outlet and the contributing cells to that puddle or the outlet.

3.1.3 Calculation of terrain parameters

Many terrain parameters, such as slope, aspect, and curvature can be derived from DEMs directly or indirectly. These computed parameters could be used to describe topography and

quantify the effect of topography on redistributing surface water, which may have significant hydrological and topographical consequences. The PD program is designed to calculate local slope and aspect of any DEM. In addition, those parameters are shown in 2D figures for better visualization.

Local slope is computed using the steepest downhill slope to one of the eight nearest neighbors (i.e., the D8 method), which is similar to determining flow directions. Local slope can be calculated as:

$$S = \max_{i=1to8} \frac{Z_0 - Z_i}{h(i)} \times 100\% \tag{18}$$

where S = local slope (%), Z_0 = elevation at the center, Z_i = elevation at the neighboring eight cells, $h(i)$ = grid size (dx) for cardinal (north, south, east, and west) neighbors (i = 1, 2, 3, 4), and $h(i) = \sqrt{2} \times$ grid size (dx) for diagonal neighbors (i = 5, 6, 7, 8). Fig. 3.3 shows the ordering of the grids for slope calculation.

Z_7	Z_4	Z_8
Z_3	Z_0	Z_1
Z_6	Z_2	Z_5

Fig. 3.3 The ordering of the grids for slope calculation

Aspect is the direction of the downhill gradient, which is calculated by the D8 method in the PD program. Aspect is measured clockwise in degrees from 0 to 360 coming full circle, which can also be described in eight directions as flow directions. Therefore, aspect is the same as flow direction in the PD program. The PD program shows aspect in eight distinct colors representing eight directions.

3.2 Applications of the Puddle Delineation (PD) Program

Since the eight surfaces in this study are characterized with hundreds of puddles with different sizes, a surface (S9) with few puddles (Fig. 3.4a) was selected here to show how the PD program calculates the MDS and NCA with more ease and clarity. Fig. 3.4b shows the puddle delineation results for S9. It can be observed that all four puddles are individually distributed as shown in Fig. 3.4a, and each puddle has one center and one threshold (Fig. 3.4b). Therefore, the MDS of each puddle can be calculated based on Eq. (17) in the PD program. Table 3.1 shows the MDS values for each puddle and the entire surface of S9. Puddle P_2 that has the highest MDS value of 9.33 cm^3 (Table 3.1) is the puddle with the largest size and depth as shown in Fig. 3.4a. Similarly, the relatively shallow and small puddle of P_3 shows the lowest MDS value of 0.77 cm^3. The MDS of the entire surface is 17.20 cm^3 by summing the MDS values of all puddles (Table 3.1).

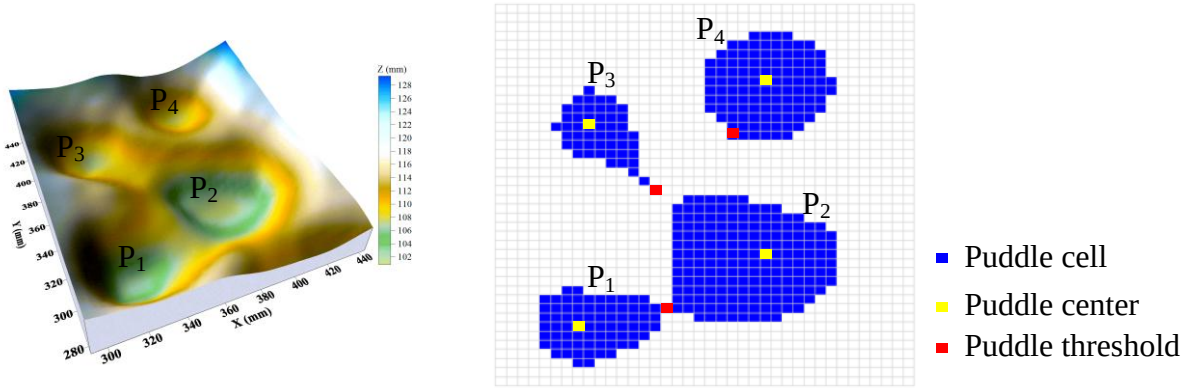

(a) Surface S9 with four puddles (b) Delineated puddles

Fig. 3.4 Puddle delineation results for surface S9

Table 3.1. The calculated MDS values for S9

	P_1	P2	P3	P4	Entire surface
MDS (cm^3)	2.86	9.33	0.77	4.24	17.20

As has been mentioned previously, the flow directions have to be determined before calculating the NCA. The calculation of flow directions has been detailed in Section 3.1.1. For better visualization, the flow directions are displayed in a 2D figure in blue lines with arrows indicating eight distinct directions. Fig. 3.5 shows the flow directions of each cell for S9. It can be seen that no flow direction is assigned to puddle centers as described in Section 3.1.1 (Fig. 3.5). The flow direction of the threshold cell can either flow into or out of the puddle based on the D8 method (Fig. 3.5).

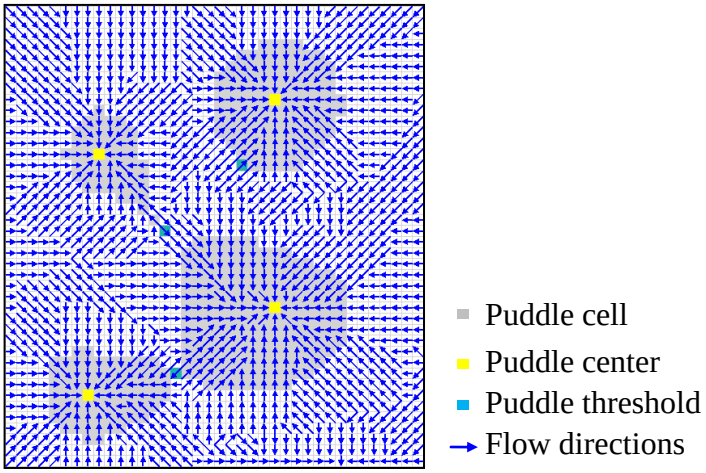

Fig. 3.5 Flow directions of S9 in 2D figure

Based on the flow directions, contributing areas for any cell can be calculated. Fig. 3.6a shows the contributing area of a puddle center for S9. It can be observed that the selected puddle center receives the water contributing from the surrounding upstream cells based on the flow directions (Fig. 3.6a). In addition, all the outlets of a surface as well as the cells that have the potential of contributing water to each outlet can be identified. In the PD program, the outlets of a surface are defined as the boundary cells with flow directions pointing out of the boundary. As has defined in section 3.1.2, each CA consists of a puddle or an outlet and the contributing cells

to that puddle or the outlet. Thus, the NCA can be determined. For example, the NCA of S9 is 5 (i.e., 5 polygons) (Fig. 3.6b).

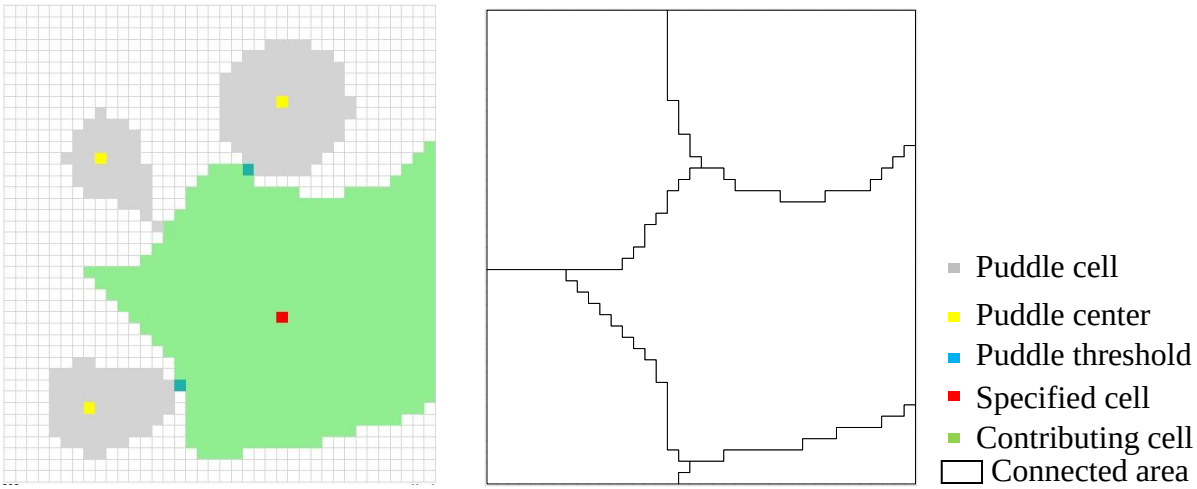

(a) Contributing area for a puddle center of S9

(b) Connected areas (CAs) and the number of CAs (NCA) of S9

Fig. 3.6 Contributing area and the number of connected areas of S9

The local slope and aspect, which determine the initial flow velocity and direction on the surface when rainfall occurs, are two of the basic surface topography parameters. They are the major factors that affect how water flows on the surface and how the drainage patterns develop on the surface. In addition, they are also important in topography related environmental and hydrologic modeling. Therefore, local slopes and aspects have been calculated to analyze surface topography in the PD program. Slope is calculated in percent rise, and aspect is measured in degrees. Since water cannot flow to anywhere else in the puddle centers, “zero” slope is assigned to the puddle centers in the PD program (Fig. 3.7a). Similarly, aspect at the puddle centers is also “zero.” The PD program shows aspects in eight distinct colors representing eight directions and additional grey color indicating the cell with “zero” aspect (Fig. 3.7b).

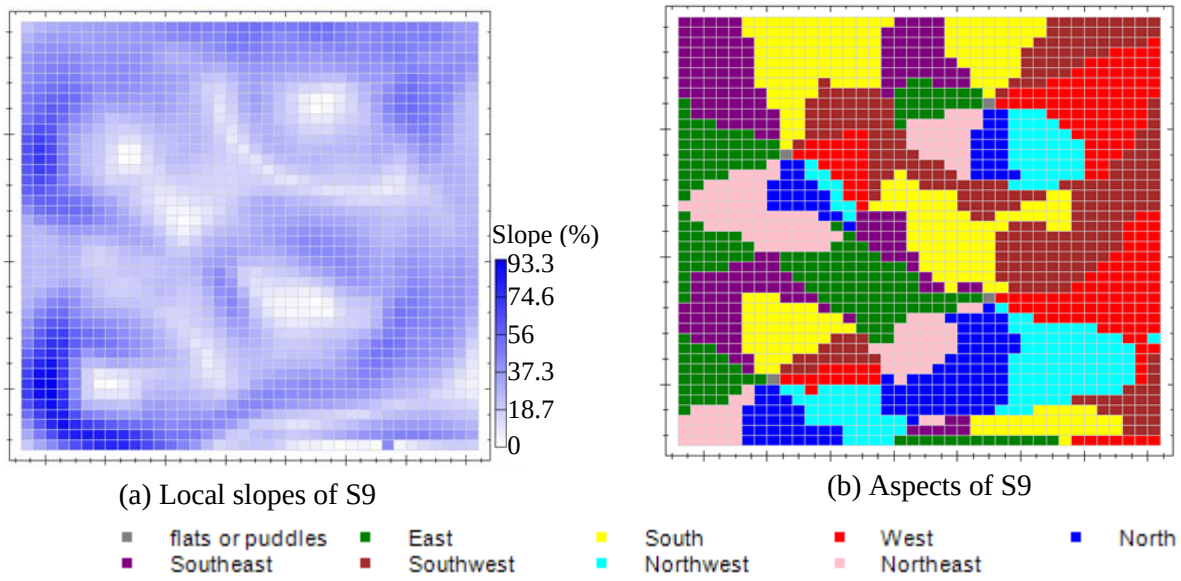

(a) Local slopes of S9

(b) Aspects of S9

Fig. 3.7 Local slopes and aspects for S9

3.3 Summary

The PD program was applied in this study to delineate surface topography, focusing on identifying puddles with any size. After puddle delineation, the MDS of each puddle as well as for the entire surface were calculated directly based on the DEM in the PD program. In addition, some of the hydrologic properties, such as flow directions and contributing areas, as well as topographic parameters such as local slopes and aspects have been computed to further analysis of surface microtopography. The NCA was determined based on the delineated puddles and the flow directions. It has been provided in this study that the PD program can effectively determine the MDS and NCA to examine surface microtopography.

CHAPTER 4. OVERALL CONCLUSIONS AND FUTURE WORK

This thesis presents results of research on the characterization of surface topography. Eight soil surfaces including six laboratory surfaces with the same area of 0.6 m $\times$ 2 m and two field surfaces with an area of 6 m $\times$ 3.2 m were selected for this research. Random roughness (RR) index and fractal parameters (D and l) were computed to characterize microtopography of those eight surfaces. The commonly-used hydrotopographic parameters, such as RR, maximum depression storage (MDS), and the number of connected areas (NCA), as well as fractal analysis provide a useful way to characterize the spatial complexity of surface microtopography.

It has been found that the RR index can quantify the overall surface roughness. The higher the RR index value, the rougher the surface is, and vice versa. Basically, the RR index is the standard deviation of the elevation changes. Therefore, the RR index lacks information on the scale effects and the spatial correlation of surface topography. To account for this issue, the fractal method has been implemented to analyze surface topography. The fractal dimension D describes horizontal roughness, which is proven to be scale dependent, and the crossover length l represents the vertical variance in elevations at the reference scale. Anisotropic properties of the surfaces were examined by using the directional semivariogram method and a modified anisotropy index (a). Furthermore, multifractal analysis was performed to identify the dissimilar changing patterns of fractal dimension (D) and crossover length (l) for the soil surfaces at different scales. It has been found that D and l at small scales describe topographic surfaces in more detail; while the overall topographic feature of the surfaces can be captured by D and l at larger scales. Surface slope removal has a great effect on the fractal calculation using the semivariogram method. This study also demonstrated that fractal parameters D and l have clear and meaningful relationships with the hydrotopographic parameters, such as RR, MDS, and

NCA. It has been found that a rough surface with a greater *D* value would have smaller RR and MDS values, and a higher NCA. Thus, the inception of surface runoff usually is delayed on the rough surface (i.e., surface with a high RR value), due to the greater MDS to be filled and more CAs (i.e., high NCA) to be hydrologically connected to contribute water to the outlet. More importantly, fractal and anisotropic analyses enable one to better understand the overland flow generation process. A surface with a small *D* value has the potential to retain more water on the surface (in depressions), which in turn redistributes surface runoff water, enhances infiltration in depressions, and delays surface runoff initiation. The dominant roughness exists along the directions of smaller *D* values. Along those directions, surface runoff is prone to be hindered/blocked by ridges, while better hydrologic connections occur along other directions, along which depressions appear to be more hydrologically connected so that the drainage networks can develop more easily.

The scale problem is critical and important in analyzing topographic surfaces. Fractal analysis can address the scale issue of a topographic surface; but this is not the focus of this thesis. Future work may further investigate the application of multifractal application in surface characterization. And efforts should be made to link the surface quantification to the modeling.

Both RR index and the fractal parameters can quantify surface microtopography statistically, but they cannot provide detailed spatial information of surfaces, such as the locations of the depressions or mounds, which is critical to hydrological analysis and modeling. The puddle delineation (PD) program applied in this study is able to spatially delineate surface microtopography. With the PD program, puddles with any size on the surface can be identified. After puddle delineation, the hydrologic properties of the surface can be determined. First, the MDS of each puddle as well as for the entire surface can be calculated. Then flow directions, and

contributing areas are determined, based on which the NCA can be effectively calculated. In addition, topographic parameters such as local slopes and aspects can be computed for further hydrologic analysis.

REFERENCES

Abedini, M. J., Dickinson, W. T., and Rudra, R. P., 2006. "On depressional storages: The effect of DEM spatial resolution." Journal of Hydrology 318 (1-4), 138-150.

Abedini, M. J., and Shaghaghian, M. R., 2009. "Exploring scaling laws in surface topography." Chaos, Solitons and Fractals 42 (4), 2373-2383.

Allmaras, R. R., Burwell, R. E., Larson, W. E., and Hotl, R. F., 1966. "Total porosity and random roughness of the interrow zone as influenced by tillage." USDA Conservation Research Report 7, 1-14.

Armstrong, A. C., 1986. "On the fractal dimensions of some transient soil properties." European Journal of Soil Science 37 (4), 641-652.

Bertuzzi, P., Rauws, G., and Courault, D., 1990. "Testing roughness indices to estimate soil surface roughness changes due to simulated rainfall." Soil and Tillage Research 17 (1-2), 87-99.

Burrough, P. A., 1983. "Multiscale sources of spatial variation in soil – I: The application of fractal concepts to nested levels of soil variations." Journal of Soil Science 34, 577-597.

Chu, X., 2011. "Characterization of Microtopography and its Hydrologic Significance." In Modeling Hydrologic Effects of Microtopographic Features, 1-14. Wang, X. (ed.), Nova Science Publishers, Inc.

Chu, X., Yang, J., and Chi, Y., 2012. "Quantification of soil random roughness and surface depression storage: methods, applicability, and limitations." Transactions of the ASABE. Under review.

Chu, X., Zhang, J., Yang, J., and Chi, Y., 2010. "Quantitative evaluation of the relationship between grid spacing of DEMs and surface depression storage." In: Challenges of Change,

4447-4457. Palmer, R. N. (ed.), Proceedings of the 2010 World Environmental and Water Resources Congress, American Society of Civil Engineers.

Currence, H. D., and Lovely, W. G., 1970. "The analysis of soil surface roughness." Transactions of the ASAE 13, 710-714.

Darboux, F., Davy, Ph., Gascuel-Odoux, C., and Huang, C., 2001. "Evolution of soil roughness and flowpath connectivity in overland flow experiments." Catena 46 (2-3), 125-139.

Darboux, F., Davy, Ph., Gascuel-Odoux, C., and Huang, C., 2002. "Effect of depression storage capacity on overland flow generation for rough horizontal surfaces: water transfer distance and scaling." Earth Surface Processes and Landforms 27 (2), 177-191.

Darboux, F., and Huang, C., 2003. "An instantaneous-profile laser scanner to measure soil surface microtopography." Soil Science Society of America Journal 67 (1), 92-99.

Darboux, F., and Huang, C., 2005. "Does soil roughness increase or decrease water and particle transfer?" Soil Science Society of America Journal 69 (3), 748-756.

Deutsch, C. V., and Journel, A. G., 1998. GSLIB. Geostatistical Software Library and User's Guide. Oxford University Press, New York, NY 369pp.

Djokic, D., 2008. Comprehensive terrain processing using ArcHydro tools. ESRI, pp. 61.

Eltz, F. L. F., and Norton, L. D., 1997. "Surface roughness changes as affected by rainfall erosivity, tillage, and canopy cover." Soil Science Society of America Journal 61 (6), 1746-1755.

Falconer, K., 2003. Fractak Geometry: Mathematical Foundations and Applications. John Wiley & Sons, Ltd.

Feder, J., 1988. Fractals. Plenum Press, New York.

Gagnon, J.-S., Lovejoy, S., and Schertzer, D., 2006. “Multifractal earth topography.” Nonlinear Processes in Geophysics 13, 541-570.

Garbrecht, J., and Martz, L. W., 1995. “TOPAZ: An automated digital landscape analysis tool for topographic evaluation, drainage identification, watershed segmentation and subcatchment parameterization: Overview.” ARS-NAWQL 95-1, 17pp., USDA-ARS, Durant, Oklahoma.

Garbrecht, J., and Martz, L. W., 1997. “The assignment of drainage direction over flat surfaces in raster digital elevation models.” Journal of Hydrology 193 (1), 204-213.

Govers, G., Takken, I., and Helming, K., 2000. “Soil roughness and overland flow.” Agronomie 20 (2), 131-146.

Green, T. R., and Erskine, R. H., 2004. “Measurement, scaling, and topographic analyses of spatial crop yield and soil water content.” Hydrological Processes 18 (8), 1447-1465.

Hairsine, P. B., Moran, C. J., and Rose, C. W., 1992. “Recent development regarding the influence of soil surface characteristics on overland flow and erosion.” Australian Journal of Soil Research 30 (3), 249-264.

Hansen, B., 2000. “Estimation of surface runoff and water-covered area during filling of surface microrelief depressions.” Hydrological Processes 14 (7), 1235-1243.

Hansen, B., Schjønning, P., and Sibbesen, E., 1999. “Roughness indices for estimation of depression storage capacity of tilled soil surfaces.” Soil and Tillage Research 52 (1-2), 103-111.

Hayashi, M., Van Der Kamp, G., and Schmidt, R., 2003. “Focused infiltration of snowmelt water in partially frozen soil under small depressions.” Journal of Hydrology 270 (3-4), 214-229.

Helming, K., Roth, C., Wolf, R., and Diestel, H., 1993. "Characterization of rainfall-microrelief interactions with runoff using parameters derived from digital elevation models (DEMs)." Soil Technology 6 (3), 273-286.

Helming, K., Römkens, M. J. M., and Prasad, S. N., 1998. "Surface roughness related processes of runoff and soil loss: a flume study." Soil Science Society of America Journal 62 (1), 243-250.

Huang, C., 1998. "Quantification of soil microtopography and surface roughness." In: Fractals in Soil Science. Baveye, P., Parlange, J. Y., and Stewart, B. A. (Eds.), CRC-Press, 153-168.

Huang, C., and Bradford, J. M., 1990. "Digressional storage for Markov – Gaussian surfaces." Water Resources Research 26 (9), 2235-2242.

Huang, C., and Bradford, J. M., 1992. "Application of a laser scanner to quantify soil microtopography." Soil Science Society of America Journal 56 (1), 14-21.

Huang, C., White, I., Thwaite, E. G., and Bendeli, A., 1988. "A noncontact laser system for measuring soil surface topography." Soil Science Society of America Journal 52 (2), 350-355.

Isaaka, E. H., and Srivastava, R. M., 1989. Applied Geostatistics. Oxford University Press, New York, NY 561pp.

Jester, W., Klik, A., Hauer, G., Hebel, B., and Truman, C. C., 2001. "Rainfall and surface roughness effects on soil loss and surface runoff." Soil Erosion for 21st Century Symposium, 463-466.

Kamphorst, E. C., and Duval, Y., 2001. "Validation of a numerical method to quantify depression storage by direct measurements on moulded surfaces." Catena 43 (1), 1-14.

Kamphorst, E. C., Jetten, V., Guérif, J., Pitkänen, J., Iversen, B. V., Douglas, J. T., and Paz, A., 2000. "Predicting depression storage from soil surface roughness." Soil Science Society of America Journal 64 (5), 1749-1758.

Klinkenberg, B., 1988. Test of a Fractal Model of Topography. PhD diss. Ontario, Canada: University of Western Ontario, Department of Geography.

Klinkenberg, B., and Goodchild, M. F., 1992. "The fractal properties of topography: a comparison of methods." Earth Surface Processes and Landforms 17 (3), 217-234.

Kuipers, H., 1957. "A reliefmeter for soil cultivation studies." Netherlands Journal of Agricultural Science 5, 255-262.

Linden, D. R., and Van Doren, D. M., Jr., 1986. "Parameters for characterizing tillage-induced soil surface roughness." Soil Science Society of America Journal 50 (6), 1560-1565.

Linden, D. R., Van Doren, D. M., Jr., and Allmaras, R. R., 1988. "A model of the effects of tillage-induced soil surface roughness on erosion." In: Tillage and traffic in crop production, 373-378. Proc. ISTRO Conf., 11th. Edinburgh, UK. 11-15 July 1988. ISTRO, Haren, the Netherlands.

Lovejoy, S., Lavallée, D., Schertzer, D., and Ladoy, P., 1995. "The $l^{1/2}$ law and multifractal topography: theory and analysis." Nonlinear Processes in Geophysics 2, 16-22.

Mark, D. M., and Aronson, P. B., 1984. "Scale-dependent fractal dimensions of topographic surfaces: An empirical investigation, with applications in geomorphology and computer mapping." Mathematical Geology 16 (7), 671-683.

Martz, L. W., and Garbrecht, J., 1993. "Automated extraction of drainage network and watershed data from digital elevation models." Journal of the American Water Resources Association 29 (6), 901-908.

Martz, L. W., and Garbrecht, J., 1999. “An outlet breaching algorithm for the treatment of closed depressions in a raster DEM.” Computers & Geosciences 25 (7), 835-844.

McClean, C. J., and Evans, I. S., 2000. “Apparent fractal dimensions from continental scale digital elevation models using semivariogram methods.” Transactions in GIS 4 (4), 361-378.

Microsoft, 2005. http://msdn.microsoft.com/en-us/library/kx37x362(v=vs.80)

Mitchell, J. K., and Jones, B. A., Jr., 1976. “Micro-relief surface depression storage: analysis of models to describe the depth-storage function.” Journal of the American Water Resources Association 12 (6), 1205-1222.

Moore, I. D., and Larson, C. L., 1979. “Estimating microrelief surface storage form point data.” Transactions of the ASAE 22 (5), 1073-1077.

Moore, D. C., and Singer, M. J., 1990. “Crust formation effects on soil erosion processes.” Soil Science Society of America Journal 54 (4), 1117-1123.

Mwendera, E. J., and Feyen, J., 1992. “Estimation of depression storage and Manning’s resistance coefficient from random roughness measurements.” Geoderma 52 (3-4), 235-250.

O'Callaghan, J. F., and Mark, D. M., 1984. “The extraction of drainage networks from digital elevation data.” Computer Vision, Graphics, and Image Processing 28 (3), 323-344.

Onstad, C. A., 1984. “Depression storage on tilled soil surfaces.” Transactions of the ASAE 27 (3), 729-732.

Pentland, A. P., 1984. “Fractal-based description of natural scenes.” IEEE Transactions on Pattern Analysis and Machine Intelligence Vol. PAM1-6 (6), 661-674.

Perfect, E., and Kay, B. D., 1995. “Applications of fractals in soil and tillage research: A review.” Soil and Tillage Research 36 (1-2), 1-20.

Planchon, O., and Darboux, F., 2002. "A fast, simple and versatile algorithm to fill the depressions of digital elevation models." Catena 46 (2-3), 159-176.

Planchon, O., Esteves, M., Silvera, N., and Lapetite, J. M., 2001. "Microrelief induced by tillage: measurement and modeling of Surface Storage Capacity." Catena 46 (2-3), 141-157.

Podmore, T. H., and Huggins, L. F., 1981. "An automated profile meter for surface roughness measurements." Transactions of the ASAE 24 (3), 663-665, 669.

Quattrochi, D. A., Lam, N. S.-N., Qiu, H. L., and Zhao, W., 1997. "Image characterization and modeling systems (ICAMS): A geographic information system for the characterization and modeling of multiscale remote-sensing data." In: Scale in Remote Sensing and GIS, Quattrochi, D. A., and Goodchild, M. (Eds.). CRC Press, Boca Raton, FL, 295-307.

Römkens, M. J. M., and Wang, J. Y., 1986. "Effect of tillage on surface roughness." Transactions of the ASAE 29 (2), 429-433.

Roy, A. G., Gravel, G., and Gauthier, C., 1987. "Measuring the dimension of surfaces: A review and appraisal of different methods." In: Proceedings: Automated Cartography (8), Chrisman, N. R. (Ed.). Baltimore, Maryland, 68-77.

SAS Institute Inc. 2009. *SAS/STAT 9.2 User's Guide, Second Edition*. Cary, NC: SAS Institute Inc.

Sun, W., Xu, G., Gong, P., and Liang, S., 2006. "Fractal analysis of remotely sensed images: A review of methods and applications." International Journal of Remote Sensing 27 (22), 4963-4990.

Sung, Q. C., Chen, Y. C., and Chao, P. C., 1998. "Spatial variation of fractal parameters and its geological implications." Tao 9 (4), 655-672.

Toy, T. J., and Foster, G. R., 1998. "Guidelines for the use of the Revised Universal Soil Loss Equation (RUSLE) version 1.06 on mined lands, construction sites, and reclaimed lands." 148 p. Available at http://www.nrcs.usda.gov/technical/ecs/agronomy/randruf2.pdf

Ullah, W., and Dickinson, W. T., 1979. "Quantitative description of depression storage using a digital surface model: I. Determination of depression storage." Journal of Hydrology 42 (1-2), 63-75.

Vázquez, E. V., Miranda, J. G. V., and González, A. P., 2005. "Characterizing anisotropy and heterogeneity of soil surface microtopography using fractal models." Ecological Modeling 182 (3-4), 337-353.

Vázquez, E. V., Miranda, J. G. V., and González, A. P., 2007. "Describing soil surface microrelief by crossover length and fractal dimension." Nonlinear Processes in Geophysics 14 (3), 223-235.

Vázquez, E. V., Vieira, S. R., De Maria, I. C., and González, A. P., 2010. "Fractal dimension and geostatistical parameters for soil microrelief as a function of cumulative precipitation." Scientia Agricola 67 (1), 78-83.

Western, A. W., Blöschl, G., and Grayson, R. B., 2001. "Toward capturing hydrologically significant connectivity in spatial patterns." Water Resources Research 37 (1), 83-97.

WMS, 2008. Watershed Modeling System, WMS v8.1 Tutorials. Aquaveo, LLC, Provo, Utah.

Xia, Z. G., 1993. The Use and Limitations of Fractal Geometry in Digital Terrain Modeling. PhD diss. New York City, NY.: City University of New York, Department of Geology and Geography.

Xia, Z. G., and Clarke, K. C., 1997. “Approach to scaling of geo-spatial data.” In: Quattrochi, D. A., and Goodchild, M. (Eds.), Scale in Remote Sensing and GIS. CRC Press, Boca Raton, FL, pp. 309-360.

Yokoya, N., Yamamoto, K., and Funakubo, N., 1989. “Fractal-based analysis and interpolation of 3D natural surface shapes and their application to terrain modeling.” Computer Vision, Graphics, and Image Processing 46, 284-302.

Zhang, W., and Cundy, T. W., 1989. “Modeling of two-dimensional overland flow.” Water Resources Research 25 (9), 2019-2035.

Zobeck, T. M., and Onstad, C. A., 1987. “Tillage and rainfall effects on random roughness: A review.” Soil and Tillage Research 9 (1), 1-20.

Zribi, M., Ciarletti, V., Taconet, O., Paille, J., and Boissard, P., 2000. “Characterization of the soil structure and microwave backscattering based on numerical three-dimensional surface representation: Analysis with a fractional Brownian model.” Remote Sensing of Environment 72(2), 159-169.